2021

Optimized Microbial Recombinant Production of HIV-1 Anti-Envelope Antibody Fragments with Applications to Single Particle Tracking of Virus Assembly

Merissa Michelle Bruns
University of Denver

Optimized Microbial Recombinant Production of HIV-1 anti-Envelope Antibody Fragments with Applications to Single Particle Tracking of Virus Assembly

_____

A Thesis

Presented to

the Faculty of the College of Natural Sciences and Mathematics

University of Denver

_____

In Partial Fulfillment

of the Requirements for the Degree

Master of Science

_____

by

Merissa Michelle Bruns

March 2021

Advisor: Dr. Schuyler Van Engelenburg

Author: Merissa Michelle Bruns
Title: Optimized Microbial Recombinant Production of HIV-1 anti-Envelope Antibody Fragments with Applications to Single Particle Tracking of Virus Assembly
Advisor: Dr. Schuyler Van Engelenburg
Degree Date: March 2021

Abstract

In my findings, I have established a set series of protocols to recombinantly produce, purify and apply various fluorescent probes *in vitro* for the fluorescent labeling and study of the human immunodeficiency virus type 1 (HIV-1) envelope (Env) protein during HIV viral assembly. There remains insufficient knowledge about the molecular dynamics and interactions of HIV-1 Env protein with its counterpart, Gag, on the inner host cell surface during assembly of a mature virus particle. There also remains an insufficient amount of data for the understanding and clarification of the mechanism of action of a known host cell HIV-1 restriction factor, Serinc5 (SER 5), which is believed to have correlation with Env in fusion events.

Using superresolution microscopy to measure and track host–pathogen interfaces that occur on a scale below the resolution limit of the light microscope is becoming increasingly popular. I have used total internal reflection microscopy (TIRF) and Photoactivated Localization Microscopy (PALM) to depict sites of molecular assembly via Env and Gag colocalization as well as measure and track other means of Env such as diffusion rates and host cell restriction factor interactions.

Overall, my findings have provided improved strategies and tools for the use in fluorescently labeling and tracking HIV-1 Env and an HIV-1 host cell restriction factor known as SER 5. Superresolution microscopy and single particle tracking can be achieved provided high specificity, brightness and purity while maintaining low K_Ds. The production and data of these probes are imperative for both understanding the pathological processes of HIV-1 assembly and other stages of the HIV-1 life cycle as well as the various protein-protein interactions.

Acknowledgments

Although this thesis will declare the discoveries, insights and results of my academic work throughout graduate school, I would first like to acknowledge that this goal was not achieved without the utmost crucial support given by many. I would first like to thank Dr. Schuyler Van Engelenburg, my Principal Investigator, for saying “yes” and giving me a chance. For accepting me as part of the team and providing me this opportunity to better myself as a scientist. For guiding me through and to my contributions in the field of HIV. I am forever grateful for joining the Van Engelenburg lab as my mind and my world have been broadened by the fascination of science that has occurred here -- keeping my inner-passion ignited and bright.

Secondly, I would like to give two special recognitions simultaneously with a heart full of gratitude to Associate Professor Dr. Dinah Loerke and Biology Lab Director Dr. Kristin Andrud. I truly cannot thank you enough for both selflessly taking on roles that were not yours, to provide essential support throughout my time here at the University of Denver. Thank you for your kindness, sympathy and graciousness during the entirety of the program. The time and effort as mentors that you have both put in have never gone unnoticed. Thank you for recognizing my stubborn personality and seeing through the “I’m okays”, noticing that every so often, support is still necessary. Thank you for reaching out and providing that to me.

How can I say “thank you” for something as immense as keys to survival and success?

I gratefully recognize my Thesis Defense Committee, Drs. Michelle Knowles, Cedric Asensio and Erich Kushner for their time, expertise, and advice.

Finally, I thank my friends and those who have supported me throughout this program. A very big thank you to Ms. Abby Altman and Mr. Nicholas Grooves for accepting me upon my arrival and for your help building a foundational beginning to my research. A bond built on the bench between lab partners often yields a lifelong memories and friendship.

Table of Contents

List of Figures

Chapter 1

Introduction

Synopsis of the HIV/AIDS Pandemic

a. The Discovery of AIDS and Initial Studies of HIV

The current year of 2021 marks the 40th tragic anniversary of the beginning of the HIV/AIDS epidemic in the United States of America. Acquired immune deficiency syndrome (AIDS) is the illness caused by the Human Immunodeficiency Virus (HIV) which has claimed the lives of over 42.2 million people globally and has recently been reported the sixth deadliest disease in the world (UNAIDS).

During the spring of 1981, the Centers for Disease Control and Prevention (CDC) in Atlanta reported a surge in *Pneumocystis carinii* pneumonia and Kaposi's sarcoma, both associated with an unknown acquired cellular immunodeficiency. The immune disorder in conjunction with the accompanying illness was soon thereafter defined as the acquired immune deficiency syndrome (AIDS). Along with *Pneumocystis carinii* pneumonia, AIDS patients were vulnerable to other life-threatening opportunistic infections, such as complications caused by the Herpes Simplex Virus. In June 1981 shortly after taking notice of the surge, the CDC began national surveillance of this novel acquired immune disorder known as AIDS, as well as the other opportunistic diseases that arose associated with AIDS. By February 1983, 1,000 cases of AIDS were reported in the USA (Jaffe, Bregman and Selik, 1983; Siegal et al., 1981).

After the AIDS had been discovered, researchers slowly began the marathon to discovery. In 1982, both doctors and researchers observed that AIDS patients' T-lymphocyte counts were (higher/lower) than those of healthy people. The depletion of the T-lymphocytes along with the

suppressed cellular immunity of these patients suggested that T cells could be a point of infection for the supposed infectious disease (Stahl et al., 1982). In 1983, another breakthrough in research occurred in Paris when researchers discovered that AIDS was associated with a virus. At the Institut Pasteur, Departement de Virologie, a retrovirus belonging to the family of human T-cell leukemia viruses (HTLVs), but unmistakably different from each previous isolate, was isolated from a patient with signs and symptoms that very commonly preceded AIDS, such as lymphadenopathy. This virus was noted to be significantly different than the previous HTLV isolates found by isolating antibodies from the patient's serum and testing reactions with proteins from viruses of the HTLV-I subgroup. The antibodies reacted with HTLV-I viral proteins, but type-specific antisera to HTLV-I did not precipitate proteins of the newly found viral isolate (Barre-Sinoussi et al., 1983). This discovered T-cell tropic behavior and the reverse transcriptase activity that confirmed a retrovirus validation won Luc Montagnier and first author, Françoise Barré-Sinoussi, the Nobel Prize in 2008 for the isolation and characterization of HIV-1.
In 1984, scientists successfully isolated HIV-1 solely from AIDS patients and were not able to isolate the virus in healthy individuals. Only months later, this team rapidly developed a cell system using a human T cell line that produced these patient's HIV-1 isolates in high yields, allowing for even further research advancement (Gallo et al., 1984; Popovic et al., 1984).

Overall, it was Montagnier's group that discovered this virus as the lymphadenopathy associated virus (LAV), it was Gallo's group that further discovered the virus as human T-cell leukemia/lymphoma virus type IIIB (HTLV-III) and in 1986 the virus was declared the Human Immunodeficiency Virus (HIV) as we now know it today (Shilts, 1987). However, 40 years post discovery, there remains a high mortality rate and a search for the cure in the absence of a vaccine.

b. Current Effects of the HIV/AIDS Pandemic

Though the discovery of HIV-1 was a tremendous breakthrough that allowed scientists to study novel medicines and treatments, suffering remains. In recent surveillance results from 2019, 25.4 million people were accessing antiretroviral therapy. 38.0 million people globally were living with HIV and 1.7 million people became newly infected with HIV. The same year, 690,000 people died from AIDS-related illnesses. Upwards of 100 million people have become infected with HIV since the start of the epidemic and 42.2 million of those people have died from AIDS-related sicknesses and their complications since the start of the epidemic (UNAIDS, 2021).

Data through June 2020 has shown a total of 26.2 million people were accessing antiretroviral therapy. In 2019, 25.6 million people were accessing antiretroviral therapy up from 6.4 million in 2009. Overall, in 2019 still only 67% of all people living with HIV were accessing treatment. Totaling all people living with HIV, 81% knew their status, 67% were accessing treatment and 59% were virally suppressed in 2019 (UNAIDS, 2021).

Medical cost estimates are often based on the health care utilization by persons with HIV/AIDS and can vary however in the U.S.A., the most recent published estimate of lifetime HIV treatment costs was $485,000 in the U.S.A (CDC, 2020).

Given these points, HIV has caused alarming damage to humanity. As HIV-1 infections rise globally, economic barriers to treatment remain despite their availability, and HIV-1 will continue to have tragic consequences.

Prevailing Treatments

a. Treatable Stages

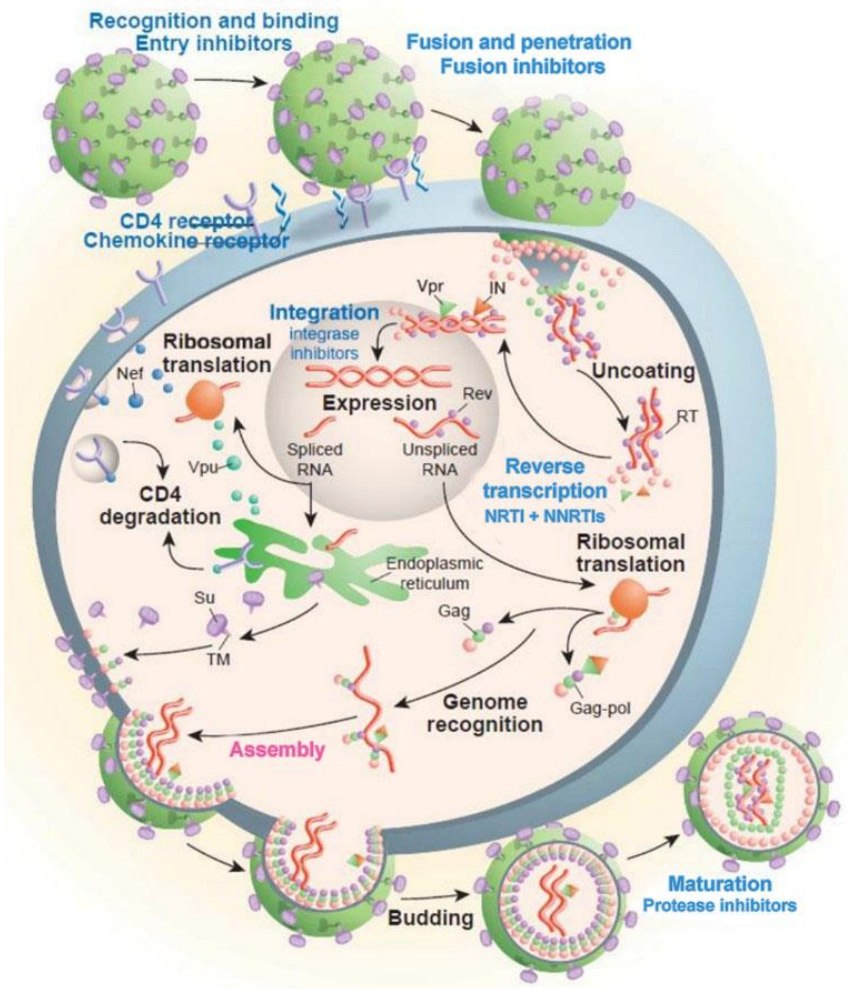

Figure 1.1 Current Antiretroviral Treatments at Various HIV-1 Infection Cycle Stages.

The text in blue labels the targets that are inhibited by existing treatments that have been approved by the FDA. Text in pink refers to the target with no current existing approved treatments. HIV follows this series of steps to multiply itself in the body. This mechanism begins when HIV interacts with a $CD4^+$ T-cell and a CCR5 co-receptor. The seven steps in the HIV life cycle are: 1) binding; 2) fusion; 3) reverse transcription; 4) integration; 5) replication; 6) assembly; and 7) budding.

This figure is modified from Pomerantz and Horn, 2003.

b. Before Highly Active Antiretroviral Therapy

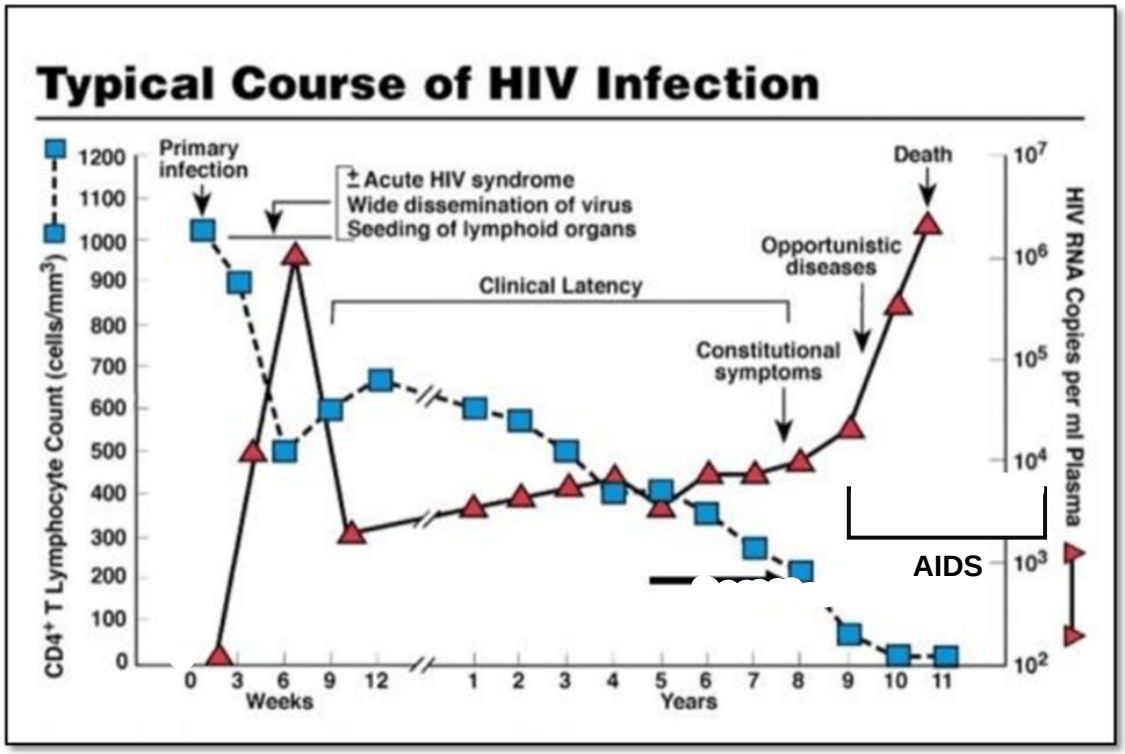

Figure 1.2. The Natural Progression of HIV After the Point of Infection (Before HAART)

The immunopathogenic mechanisms of HIV without ARVs include the steady decrease in the host's $CD4^+$ immune cells while overlapping with a steady increase in viral RNA copies. For the entirety of an HIV infection, immunodeficiency progresses. Immunodeficiency begins to decline even while the disease symptoms are not present—Clinical Latency Period. At the point of expressing inherent symptoms of an HIV infection, the patient is diagnosed with AIDS. Adapted and modified from Fausi *et al*., 1996

c. HAART/ARVs

Table 1: FDA-Approved Drug Classes of HIV-1 ARV's

DRUG CLASS	MODE OF ACTION (M.O.A)	FIRST AUTHORIZED DRUG	APPROVAL DATE
Nucleoside Reverse Transcriptase Inhibitors (NRTIs)	HIV reverse transcriptase is inhibited both by competing with the natural substrate, deoxyadenosine 5'-triphosphate, and by its incorporation into viral DNA causing termination of viral DNA chain elongation.	Zidovudine (AZT)	March 19, 1987
Protease Inhibitors (PIs)	**Inhibits HIV protease, enzymes that cleave viral proteins needed for maturation and replication.**	**Saquinavir**	**December 6, 1995**
Nonnucleoside Reverse Transcriptase Inhibitors (NNRTIs)	HIV reverse transcriptase is inhibited by direct binding and inactivation of the enzyme.	Nevirapine	June 21, 1996
Fusion Inhibitors	**Blocks fusion from occurring, therefore preventing HIV entry into CD4 cells.**	**Enfuvirtide**	**March 13, 2003**
CCR5 Antagonists	Blocks CCR5 receptors on CD4 positive cell surfaces, therefore preventing HIV entry into CD4 cells.	Maraviroc	August 6, 2007
Integrase Strand Transfer Inhibitors (INSTIs)	**Inhibits integrase, an enzyme requires for integrating viral DNA into the Human host genome.**	**Raltegravir**	**October 12, 2007**
Post Attachment Inhibitors	Reduces viral load by preventing viral progeny from re-attaching to uninfected host cells. Used in HTE patients.	Ibalizumab-uiyk	March 6, 2018
gp120 attachment inhibitor	**Locks gp120 into a closed state that prohibits the conformational change necessary for interaction between the virus and the surface receptors on CD4 cells, therefore preventing attachment and entry into host T cells and other immune cells; has no in vitro cross-resistance with other classes of antiretroviral drugs therefore, used with MDR HIV strains.**	**Fostemsavir**	**July 2, 2020**

ARV: antiretroviral; CCR5 C-C Chemokine Receptor type 5; HIV: Human Immunodeficiency virus; HTE: Heavily Treatment-Experienced; MDR: Multidrug Resistant

Reference(s): Pan et al., 2008; Arts and Hazuda, 2012; Chaudhuri et al., 2018; Kpzal et al., 2020; https://www.accessdata.fda.gov/

HIV Infection Cycle

a. Retroviruses and an Overview

HIV-1 belongs to the *Retroviridae* family and is typical of other retroviruses in life cycle behavior. Retroviruses are classified by their use of reverse transcriptase and their genomic RNA. An overview of retrovirus life cycle behavior consists of the virion that binds to host target cells via specific interactions between the viral envelope with receptors on the target host cells. The final product is progeny virions that bud off from the host cell plasma membrane, completing the reproductive cycle.

b. Binding-Replication

The first events of infection are known as fusion and entry. In order to enter the host cell, the virus requires at least 2 receptors —the CD_4 molecule and a coreceptor, a chemokine receptor, such as CCR4 or CRCX5 (Choe et al., 1996). During membrane fusion, the virus is first introduced into the naïve host cell via the binding of the viral envelope glycoprotein gp120 to CD_4 on the targeted host cell. Upon binding, this will induce a conformational change in gp120 which yields a binding site for the chemokine receptor (Pier, 2004). The exposed binding site on gp120 will then bind the chemokine receptor in the human host cell, inducing yet another conformational change to the correlative gp41. After the conformational change occurs in gp120, it then disengages from gp41 so that the fusion peptide can be inserted into the target plasma membrane (Furuta et al., 1998). The mechanism of insertion and fusion can be explained by the formation of a heat stable 6 helix bundle which drives this event (Melikyan et al., 2000). Upon fusion of gp41 with the targeted cell plasma membrane, the membrane is spanned by the helix complex and the viral core, capsid (CA), is released into the cytoplasm of the targeted human host cell where it then makes its way towards the nucleus. Upon CA entry, uncoating of the core's subunits take place and interactions with host cell factors then begin as well as trafficking of the viral genome to the nucleus (Ambrose & Aiken, 2014). CA encases the viral RNA genome, reverse transcriptase, integrase, and proteases. Consequent to nucleus entry the viral RNA

contained within the core is reverse transcribed into viral DNA via reverse transcriptase (Pier, 2004). Reverse transcriptase is an RNA dependent DNA polymerase and combined with the 2 copies of single-stranded RNA genome will synthesize a single strand of DNA complementary to this viral RNA. Rnase H will then degrade this viral RNA, which then allows for synthesis of the second strand of DNA yielding double-stranded viral DNA (Pier, 2004). The viral ds-DNA translocates to the nucleus and is integrated via integrase into the host's nuclear chromatin. At this point, the human host's genome has now been "hijacked" by HIV. An important player to note during this stage is Rev, a protein of HIV-1 that goes back and forth between the nucleus and cytoplasm and contains a nuclear localization signal and a nuclear export signal, respectively and its primary function is nuclear import and export (Pollard & Malim, 1998). The virus can now use the machinery of the infected host cell containing integrated viral DNA, to create the building blocks for progeny virus. This stage is called replication within the HIV life cycle and is the last stage at which treatment exists for.

c. Assembly and Maturation

As mentioned above, the machinery of the infected host cell will be used by the virus from replication and proceeding steps. The newly formed viral DNA gests transcribed by commandeered host RNA polymerase II into splice-able full-length viral RNA (Purcell & Martin, 1993). The nuclear protein Rev comes into play again and exports this newly transcribed viral RNA out of the nucleus and into the cytoplasm to serve as mRNA for translation into viral proteins. On a free ribosome, the gag glycoprotein precursor, Pr55Gag, is translated and produces Gag along with all of its structural components: matrix (MA), capsid (CA), nucleocapsid (NC) along with the P6 domain and 2 spacer peptides SP1 and SP2 (Adamson & Freed, 2007). The C-terminus of CA contains the protein dimerization interface while MA binds to the inner leaflet of the plasma membrane and oligomerizes to create a lattice (Mailler et al., 2016). Binding of MA to the host cell's plasma membrane is driven by the post translational modification, known as myristylation, at the N-terminus. Myristylation allows for hydrophobic interactions with

membranes and the highly basic region at the surface of the membrane, which allows for electrostatic interactions with cellular lipids and membrane markers such as phosphatidylinositol-4,5-bisphosphate (Chen et al., 2014; Olety & Ono, 2014). Plasma membrane association of the structural protein Gag, depends on its myristoylated matrix domain and this plasma membrane marker $PI(4,5)P_2$. (Mücksch *et al*., 2017).

Glycoprotein (gp) 160 is the primary Envelope glycoprotein complex gene product and it is cleaved by cellular protease furin, into gp120 and gp41 (Veronese et al., 1985). Env trafficks through the secretory pathway to the plasma membrane where it is displayed on the surface, gp120, and transmembrane protein, gp41 (Adamson & Freed, 2007). There are various models proposed for how Env and Gag interact at the surface to form a viral particle.

Along with Env and Gag, the genomic RNA also needs to be recruited to sites of assembly for packaging into progeny virions. Single-molecule tracking via live cell fluorescence microscopy has shown that in the absence of Gag, the genomic viral RNA diffuses randomly within the cell, proving that it is not actively transported through the cytoplasm and that in fact, the RNA relies on Gag to traffic to the plasma membrane (Chen et al., 2014).

After all required components have been recruited to the plasma membrane, the virus can now form a bud and be released from the plasma membrane. The PTAP motif in Gag allows the recruitment of Tsg101 and other ESCRTs to virus assembly sites where they mediate budding (Strickland et al., 2017). Tsg101 and ESCRT proteins are the players present to allow for the pinching off the bud so that it can be released into the host's blood stream for new infections.

The final stage of the viral life cycle of HIV-1 is known as maturation which occurs after assembly and release from host cells. Maturation is primarily comprised of morphological rearrangements of the virus particle forming the structural core and stabilizing the 2 strands of RNA (Sundquist & Kräusslich, 2012). The viral protease will cleave the Pr55Gag and Pr160Gag–Pol precursors producing the structural components required for a new infection cycle. Once a

mature particle has formed, the cycle begins anew and gp120 then binds to CD4 on a new host cell and fusion and entry occur again.

Fluorescent Labeling

a. Modern State of the Art Strategies

The microscope and light microscopy have allowed researchers the ability to visualize molecular details in biological systems since the 16th century however, superresolution microscopy has more recently overcome a resolution boundary known as the diffraction limit of light. Superresolution imaging has frequently and rapidly been evolving and can be applied to image cellular structures and protein-protein interactions in three dimensions, multiplex coloring, and single particle tracking in living systems with resolution down to a nanometer scale. More specifically, superresolution microscopy has been used to address the organizational structure, interaction, stoichiometry and dynamics of HIV-1 and several components involved in infected cells and tissues (Muranyi *et al*., 2013; Iliopoulou *et al*., 2018; Inamdar; 2019)

Fluorescent superresolution microscopy has been crucial in the evolution of understanding the molecular and structural interactions as well as organizations of biological systems. With high molecular specificity and multi-color use capabilities, direct interactions can be seen between specifically labeled molecular species by observing co-localizations, distances, confirmation states etc. With low invasiveness, fluorescent superresolution microscopy serves as a perfect candidate for live cell imaging and the study of living systems (Sigal *et* al., 2018).

To overcome the diffraction limit, the ability to distinguish molecules that reside within the same diffraction-limited volume is required (Sigal *et* al., 2018). Stochastic Optical Reconstruction Microscopy (STORM) is one technique used to overcome the diffraction limit of the Point Spread Function (PSF) of molecules that are being tracked, located, or measured. When two identical fluorophores are spaced apart in the lateral plane, also known as the x-y plane, and the distance

is greater than the diffraction limit these two spots can be differentiated and resolved. If they are too close then these fluorophores cannot be tracked separately and are overlapped (Pawley, 2006). This then explains that the resolution of the microscope is limited by the width of the PSF and images that are under the PSF are unresolvable as single molecules, appear to be blurry and their localization cannot be correctly determined (Bates *et al.,* 2013).

b. Desirable Properties of a Molecular Probe

To use STORM, a molecular probe must have the feature of photoswitchability—the ability to go between fluorescent and dark states and this must be controlled. If the entire population of probes switched on and off at the same time, then the same resolution issue would remain or lack thereof the ability to resolve. A cycle of activation, localization, deactivation, and plotting is performed repeatedly in order to determine resolved localizations of the blinking fluorophores (Bates et al., 2013). A high-resolution image can then be reconstructed from all of the plots and localization points collected during imaging and is no longer subjected to limitations by the diffraction limit of light however, it is limited to the number of photons collected and the amount of fluorophores that are actually labeling the sample (Thompson et al., 2004).

Quantum yield is the measurement of the probability of the probe absorbing 1 photon and returning that photon back—the value of 1 being a complete return of photons. Therefore, the higher the quantum yield the better chances the molecular probe will not be dark.

Another trait is the molar extinction coefficient (ε); depicting how well the chosen fluorophore absorbs at its peak wavelength. The product of the quantum yield and the molar extinction coefficient yields the brightness of the probe (Lakowicz, 2006). These traits are important to the precision of each measurement in STORM because your precision is determined by the number of photons outputted from the activated fluorophore during a single cycle of blinking on and off (Bates et al., 2013). The less the number of photon output from your probe, the dimmer it will be

and vice versa which beautifully demonstrates the correlative product of quantum yield and molar extinction coefficient amounting to brightness.

Due to the phenomenon of fluorescence, all fluorophores are excited and emit at different wavelengths, known as peak wavelengths, giving rise to the diversity of the selection of probes that can be used and this can be helpful to the researcher for reasons such as multiplexing. With the diversity of the visible light spectrum emitted from the fluorophore of choice, comes variability in the excitation wavelength as well. High-intensity light can be damaging to the cell itself and can also be phototoxic to the fluorophore. The main phototoxic effect is the result of the fluorophore becoming photobleached. Fluorophores cannot be excited unlimitedly and each time the probe is illuminated, a fraction of the population will be permanently destroyed. Photobleaching, in general, cannot be avoided and is the limiting reagent that determines how many images can be acquired (Ettinger & Wittmann). Another limiting factor of photobleaching is the rate at which the fluorophore is bleached, also known as its photostability (Simonson et al., 2011). Photobleaching is not equivalent to photoswitchability of probes and is not turning them off, or switching to the dark state.

Duty cycle is also an important factor to consider among molecular probes, depending on the microscopy technique approach. When using techniques that require a blinking probe, it is important to note that the probe will not be entirely in its on state or its off. Duty cycle refers to how long a fluorophore is in its on state/excited state in relativity to its dark state and the most ideal fluorophore can only be used once (Tam et al., 2014).

Chapter 2

Monoclonal Antibody Fragment: BG18

Sources and Properties

In search for broadly neutralizing antibodies used to control and reduce viremia, researchers recruited donors whose serum was monitored for neutralization of HIV over a period of time. Individuals develop antibodies after many years of chronic infection and only in 10-20% of infected people (Yacoob *et al.,* 2016). A collaborative vaccine-based research group gathered a population of HIV-1 positive donors for this type of ELISA study and discovered BG18 in 2006. Donor EB354 received an HIV-1 diagnosis in 1986 and their antibodies were purified and first tested for neutralization starting in 2006 when the viral load was significantly lower than years previously documented (<400 copies/ml). At the end of this trial, 152 antibodies were found and formed 22 clones. Antibodies from 3 of the 22 clones were found to have the highest tier rating of neutralization activity. The 3 clones were then assessed further, and discovery revealed that antibody BG18 accounted for much of the serologic activity and the other 2 antibodies were significantly less potent (Freund *et al*., 2017). To date, BG18 is referred to as the most potent bnAb located at the N332-supersite (Steichen *et al.*, 2019)

Upon genomic comparison, BG18 was found to be very closely related to 2 previously isolated bNAbs directed against the V3 region of Env. The anti-Env antibodies related to BG18 are 10-1074 and PGT121 (Mouquet *et al*., 2012; Caskey *et al*., 2017). The PGT121/10-1074 family grouped the newly found BG18 into the V3/N332$_{gp120}$ class of HIV-1 bNAbs (Walker *et al*., 2011). This specific class of antibodies, including BG18, recognize both protein and glycan components on Env allowing for neutralization of most HIV-1 strains (Garces *et al*., 2015; Sok *et al*., 2016; Doores *et al*., 2015). BG18's binding site on Env involves its CDR H3 loops, which

interact with the $N332_{gp120}$ glycan and breaks through the glycan shield to also interact with a conserved peptide motif, GDIR, near the base of the V3-loop on the Env gp120 ectodomain (Pejchal *et al.,* 2011; Gristick *et al*., 2016).

To further understand BG18's binding properties, a crystallization structure of BG18 has been solved. An X-ray free electron laser was used to overcome the limitations of crystal size and improve the resolution to 3.8 Å for a BG18-BG505-35O22 complex. BG18 and 35O22 were both in the fab form upon binding the BG505 Env in a trimer state. BG18 showed more protein surface contact with Env than any other PGT121-like antibodies (Barnes *et al.,* 2018). Depicting the crystal structure of the BG18 fab has allowed for the reveal of an immunogenic epitope as well as a desirable target for a fluorescent probe. BG18 would be a preferable fab for the use of tracking HIV-1's Env over a fab such as 35O22, because of its ability to bind to the outermost part of Env's ectodomain on gp120 as opposed to the sterically hindered gp41 interface.

Previously mentioned, it is important for a fab to contain a high affinity, or a low Kd value, when used in tracking methods. A binding assay for BG18 was performed at which complete BG18 Fab was captured in a 3-fold dilution series starting at 110 nM at 30 µL/s for 60 s and permitted to dissociate for 300 s against 8ANC195 IgG, a gp120-gp41 interface bNAb. Kinetic analyses allowed for the reveal of the *ka*, *kd*, and KD values for a 1:1 binding ratio (Barnes *et al.,* 2018). It was found the BG18 has a kd of 4 nm (Freund *et al*., 2017). This is a native BG18 kd to an HIV-1 Env trimer however, in a HIV vaccine design study, BG18 containing a mutation within the CDR H3 loop bound an Env trimer with a K_D of near 2 pM (Steichen *et al.*, 2019). The highlighted traits of BG18 such as its high affinity for HIV-1 Env's gp120 N332 glycan, gives it a significant increase in desirability as an Env tracking probe.

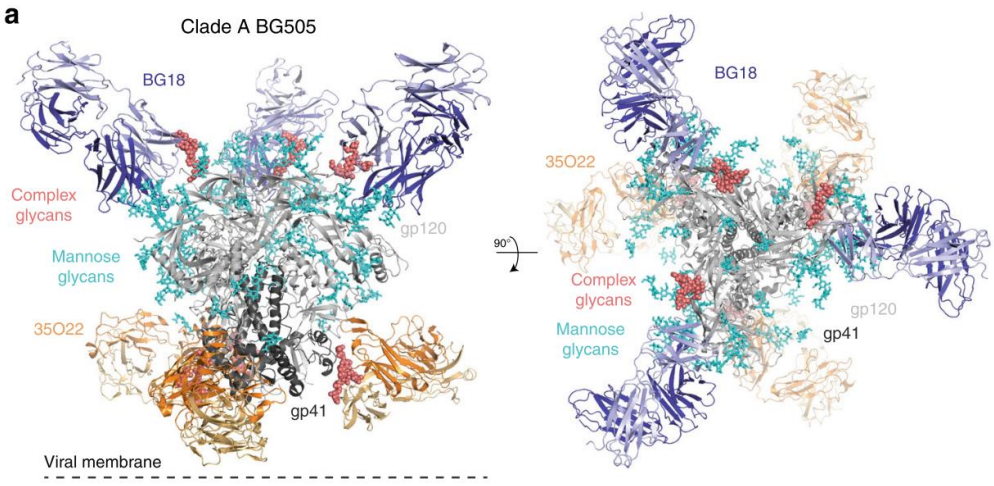

Figure 2.1. Cartoon portrayal of a crystal structure of natively glycosylated HIV-1 Env trimers bound with BG18.

Cartoon representation of a formation of a clade A Env (gp120, light gray; gp41, dark gray) bound with BG18 Fab. High-mannose glycans (cyan) are represented as sticks, and complex-type glycans (salmon) are shown as spheres Figure adapted from Barnes *et al*., 2018.

Materials and Methods

a. Cloning of BG18 Fab

The pCOMB-3H-b12 plasmid is digested with SacI and NotI restriction enzymes for 12 hours at 37℃ and purified using a Monarch Gel Extraction Kit (NEB). BG18 light chain and heavy chain antibody amino acid sequences are accessible from the Protein Data Bank (PDBID: 6CH9) [Barnes et al.]. The fragment containing BG18 antigen binding sequences were synthesized (IDT; Coralville, IA, USA) and cloned into the pCOMB3H-b12 vector using *SacI* and *NotI* sites, replacing the b12 fab coding sequence (Barbas *et al*., 1994). The pIII region of BG18 Heavy and Light chain genes were amplified from a designed gBlock (IDR) with primers carrying SacI and NotI sites, containing pCOMB homology. Amplicons were ligated via Gibson reaction into the opened pCOMB vector. All sequencing was confirmed and validated through Quintara Biosciences.

b. Test Expressions

Immediately following DNA sequence validation, transformation of the pCOMB-3H-BG18 plasmid is performed in *Escherichia Coli* XL1 Blue competent cells (Stratagene; San Diego, CA, USA). This strain is plated on LB agar containing the selective antibiotic, carbenicillin, and incubated overnight for approximately 16-18 hours at 37°C. A population of bacterial colonies (n>6), is selected for and each colony is inoculated into 1 X 5 mL LB broth media containing carbenicillin (100 µg/ml), tetracycline (15 µg/ml) and dextrose (.02 M). Incubation then occurs overnight at 37°C in a shaking incubator at ~220-250 RPM. After 16-18 hours, observe cultures to ensure a moderate amount of growth and biofilm production. Measure the OD_{600} and select for the culture amongst the population that nears the OD_{600} of 0.3 A. Once the ideal culture has been determined, discard the remainder of the population. The entire 5 mLs of the overnight culture will then be used to inoculate 2 x 50 mL Super Broth medium containing carbenicillin (100 µg/ml) and

tetracycline (15 µg/ml) in a 250-mL flask for appropriate aeration and 2 x 50 mL Luria Broth medium containing carbenicillin (100 µg/ml) and tetracycline (15 µg/ml) in a 250-mL flask for appropriate aeration. To inoculate, spin 5 mL cultures at 4,000 xg for 5 minutes, pour off and discard the supernatant and vortex pellet with 1 mL of Phosphate-Buffered Saline, pH 7.4 (PBS). Repeat this PBS cell wash step 3 times. After discarding the final wash supernatant, 1 mL of LB is added to the pellet which is then vortexed thoroughly. 250 uLs of vortexed culture is then added to the 50 mLs of SB and LB broth flasks and swirled to mix evenly. Cultures are then grown at 37°C until mid-log phase of growth (OD_{600} is approximately 0.6 A) which is a timed averaged of approximately 8 h After mid-log phase has been reached, 2 of the flasks will be removed from the 37°C and placed into a 30°C shaking incubator with equivalent RPM. Cultures are then shaken and grown overnight for 16-18 h The cells are harvested by normalizing the OD_{600} to the limiting culture and then pouring the cultures into 50 mL conical tubes and spun for 20 min at 6,000 x g using a Fiberlite F13-14 x 50cy Fixed-Angle rotor in a Sorvall centrifuge (Thermo Scientific). The pellet is then washed (3 X 30 mL [1X] PBS). Store the pellet at -80°C for at minimum of 1 hour. *Note: storage time can be up to 1 year*.

Cellular lysates were produced by sonication in PBS pH 7.4 supplemented with 0.2 mM PMSF (Gold Biotechnology). Soluble proteins were clarified via centrifugation at 30,000× *g* for 30 min and filtration by 0.22 µm cellulose acetate syringe filter. Use a large probe, preferably the 300w Ultrasonic Homogenizer sonicator with the following settings: cycle 40% output power 1 minute ON and 4 minutes OFF (Vevor). Centrifugation was performed using the same Fiberlite F13-14 x 50cy Fixed-Angle rotor in a Sorvall centrifuge (Thermo Scientific). *Note: It is very important at this step to ensure your centrifuge balance is equivalent in mass to that of the sonicated lysate.* Cell lysates can now be analyzed.

c. Western Blot

After lysis, proteins are loaded and separated by a 13% polyacrylamide gel and transferred to a methanol activated PVDF membrane (GE Healthcare). The membrane is blocked for 24 hours at 4ºC in PBSTM containing 5% milk and immediately probed overnight at 4ºC with gentle rocking. After 1-hour incubation with human-anti-Lclambda-HRP (Abcam), the protein levels are detected with SuperSignal Dura Luminol reagents (Thermo Scientific).

d. Scale-up: Production of BG18 (1L)

Construct used: N-terminal Light Chain gene with C-terminal His-6 tag on Heavy Chain in a pCOMB vector (ampicillin/carbenicillin resistance).

Construct name: pCOMB3H-[BG18frz]

The construct is newly transformed into *E. coli* XL1Blue cells or plated from a glycerol stock of freshly transformed XL1Blue cells (Stratagene; San Diego, CA, USA). The cells are plated out on LB-agar containing ampicillin (100 µg/ml) and tetracycline (15 µg/ml). Incubation then occurs overnight for 16-18 h at 37°C. A colony is selected from the plate to inoculate 1 X 5 mL LB medium containing carbenicillin (100 µg/ml), tetracycline (15 µg/ml) and dextrose (.02 M). Incubation then occurs overnight at 37°C in a shaking incubator between 220-250 RPM. At the point of overnight growth after , the 5 mL culture will then be used to inoculate 1 x 1 L Super Broth medium containing carbenicillin (100 µg/ml) and tetracycline (15 µg/ml) in a 2-L flask for appropriate aeration. After 16-18 hours, observe culture to ensure a moderate amount of growth and biofilm production. Measure the OD_{600} of culture and make note for future optimization. Ideal OD_{600} is approximately 0.3 A. The entire 5 mL of the overnight culture will then be used to inoculate 1 x 1 L SB broth medium containing carbenicillin (100 µg/ml) and tetracycline (15 µg/ml) in a 2 L flask for appropriate aeration. To inoculate, spin 5 mL culture at 4,000 xg for 5 minutes, pour off and discard the supernatant and vortex pellet with 1 mL of PBS. Repeat this PBS cell wash step 3 times. After discarding the final wash supernatant, 1 mL of LB is added to the pellet which is then vortexed thoroughly. The entire 1 mL of vortexed culture is then added via pipette to

the 50 mLs of SB broth and swirled to mix evenly. Cultures are then grown at 37°C until mid-log phase of growth (OD_{600} is approximately 0.6 A) which is a timed averaged of approximately 8 h After mid-log phase has been reached, the flask will be removed from the 37°C and placed into a 30°C shaking incubator with equivalent RPM. Cultures are then shaken and grown overnight for 16-18 h Harvest is performed by pouring the cultures into 500 mL centrifuge bottles and spun for 20 min at 6,000 x g using a Fiberlite F13-14 x 50cy Fixed-Angle rotor in a Sorvall centrifuge (Thermo Scientific). The pellet is then washed (3 X 30 mL [1X] PBS) and recollected into a 50 mL conical tube. Store the pellet at -80°C for a minimum of 1 hour. *Note: storage time can be up to 1 year*.

Cellular lysates were produced by sonication in PBS pH 7.4 supplemented with 0.2 mM PMSF (Gold Biotechnology). Soluble proteins were clarified via centrifugation at 30,000× *g* for 30 min and filtration by 0.22 µm cellulose acetate syringe filter. Use a large probe, preferably the 300w Ultrasonic Homogenizer sonicator with the following settings: cycle 40% output power 1 minute ON and 4 minutes OFF (Vevor). Centrifugation was performed using the same Fiberlite F13-14 x 50cy Fixed-Angle rotor in a Sorvall centrifuge (Thermo Scientific). *Note: It is very important at this step to ensure your centrifuge balance is equivalent in mass to that of the sonicated lysate.* Cell lysate now contains solubilized BG18 to be purified via CaptureSelect CH1-XL affinity chromatography resin (Thermo Scientific; Waltham, MA, USA).

e. Incorporated Unnatural Amino Acid Production (1 L)

Construct(s) used: N-terminal Light Chain gene with C-terminal Amber- His-6 tag on Heavy Chain preceding Ochre in a pCOMB vector (ampicillin/carbenicillin resistance).

And a tRNA/tRNA synthetase pair for the *in vivo* incorporation of the negatively charged unnatural amino acid, p-azido-l-phenylalanine, onto BG18's heavy chain in *E. coli* response to the Amber stop codon, encoded in a pEVOL vector (chloramphenicol resistance).

Construct(s) name: pCOMB3H-BG18-LC-Amber-His6-Ochre and pEVOL-pAzF [1].

The constructs are newly co-transformed into *E. coli* XL1Blue cells or plated from a glycerol stock of freshly transformed XL1Blue cells (Stratagene; San Diego, CA, USA). The cells are plated out on LB-agar containing ampicillin (100 µg/ml), tetracycline (15 µg/ml) and chloramphenicol (33 µg/ml). Incubation then occurs overnight at 37°C. A colony is selected from the plate to inoculate 1 X 10 mL LB medium containing carbenicillin (100 µg/ml), tetracycline (15 µg/ml), chloramphenicol (33 µg/ml) and a final concentration of .02 M dextrose. Incubation then occurs overnight for 18-18 h at 37°C in a shaking incubator at 220-250 RPM. The entire 10 mL of the overnight culture will then be used to inoculate 1 x 1 L SB broth medium containing carbenicillin (100 µg/ml), tetracycline (15 µg/ml) and chloramphenicol (33 µg/ml) in a 2 L flask for appropriate aeration. To inoculate, spin the 10 mL starter culture at 4,000 xg for 5 minutes, pour off and discard the supernatant and vortex pellet with 5 mL of PBS. Repeat this PBS cell wash step 3 times. After discarding the final wash supernatant, 1 mL of LB is added to the pellet which is then vortexed thoroughly. The entire 1 mL of vortexed culture is then added via pipette to the 1 L of SB broth and swirled to mix evenly. Cultures are then grown at 37°C until mid-log phase of growth (OD_{600} is approximately 0.6 A) which is a timed averaged of approximately 5 h After mid-log phase has been reached, 1 mM 4-Azido-L-phenylalanine (pAZF) was supplemented to the culture and expression of unnatural tRNAs and synthetase was induced with 2% (w/v) L-arabinose (Gold Biotechnology; St. Louis, MO, USA). Cultures are then shaken and grown overnight for 16-18 h Harvest is performed by pouring the cultures into 500 mL centrifuge bottles and spun for 20 min at 6,000 x g using a Fiberlite F13-14 x 50cy Fixed-Angle rotor in a Sorvall centrifuge (Thermo Scientific). The pellet is then washed (3 X 30 mL [1X] PBS) and recollected into a 50 mL conical tube. Store the pellet at -80°C for a minimum of 1 hour. *Note: storage time can be up to 1 year*. BG18 fab that successfully suppressed the amber stop codon with pAZF was purified using Nickel affinity chromatography (Gold Biotechnology) followed by purification using CaptureSelect CH1-XL affinity chromatography resin (Thermo Scientific; Waltham, MA, USA).

Elution fractions were pooled and dialyzed overnight in PBS, pH 7.4. Expression was assessed by SDS-PAGE analysis on 4–20% gradient gel (Bio-Rad; Hercules, CA, USA). The final yields from 1–2 L of culture were typically in the range of 1–3 mg of BG18-pAzF.

pEVOL-pAzF was a gift from Peter Schultz (Addgene plasmid #31186).

f. Ni^{2+} Polyhistidine Affinity Chromatography Purification

Cell lysis is to be performed in Buffer A, a solution adjusted to pH 8.0 containing 20 mM HEPES, 300 mM NaCl, 300 mM KCl and 20 mM imidazole. The Ni^{2+} resin is then equilibrated with Buffer A and batch incubated with the lysate over ice. To batch incubate, use desired amount of resin and resuspend 1 mL Buffer A and combine with cell lysate in 50 mL conical tube and rock slowly on ice for ≥ 1 h. Using a drip column, the resin is poured slowly to pack the column while the flowthrough is collected for future analysis. Wash the column with 12 column volumes of Buffer A solution, occasionally collecting flowthrough fractions for analysis. To elute, use 5 mL Buffer A containing 250 mM imidazole, collecting 1 mL fractions in 1.5 mL Eppendorf tubes. Elution fractions were pooled and dialyzed overnight in PBS, pH 7.4 with SnakeSkin dialysis tubing at 4°C (Thermo Scientific). Expression is assessed by SDS-PAGE analysis on 4–20% gradient gel (Bio-Rad; Hercules, CA, USA). Protein concentration can also be analyzed by calculating the absorbance at 280 nm and utilizing the Beer-Lambert Law.

g. CH1-XL Affinity Chromatography Purification

Create and pack a 0.5 mL resin bed of CaptureSelect CH1-XL affinity chromatography resin (Thermo Scientific; Waltham, MA, USA) in a Flex Column, equilibrated to room temperature with running buffer (Kimble). Running buffer consists of [1X] PBS, pH 7.4, .05% (v/v) TWEEN and .05% w/v sodium azide. Pour 20 mL cell lysate at a time over the resin bed carefully collecting the flowthrough. The column is washed with ≥ 300 mL running buffer before eluting the protein while simultaneously collecting flowthrough fractions. Ensure that the flow rate of running buffer does

not exceed 2 mLs/min. To elute the protein from the column, 5 mL .2 M glycine at a pH of 2.2 is slowly poured over the matrix and neutralized in 1 M Tris pH 9 to yield a collected fraction at a neutral pH of 7.4. *Note: volume of the fraction is variable based entirely on preference.* Elution fractions were pooled and dialyzed overnight in PBS, pH 7.4 with SnakeSkin dialysis tubing at 4°C (Thermo Scientific). Expression is assessed by SDS-PAGE analysis on 4–20% gradient gel (Bio-Rad; Hercules, CA, USA). Protein concentration can also be analyzed by calculating the absorbance at 280 nm and utilizing the Beer-Lambert Law.

h. DIBO Cu-free Click Reaction

Copper-free click chemistry was performed between DIBO-QD625 (Site-Click kit, Thermo Scientific) and BG18-pAzF using a 1:1.5-fold stoichiometry, respectively. The reaction could proceed for 12–18 h at room temperature in the dark. Uncoupled DIBO-QD625 was removed from the reaction by another round of CaptureSelect CH1-XL affinity chromatography. Elution fractions were pooled and unreacted BG18-pAzF, lacking a DIBO-QD625 conjugate, was removed by filtration through a 100 Kda molecular weight cutoff filter (Site-Click kit) followed by repeated buffer exchanges with PBS, pH 7.4.

i. Acknowledgments

pEVOL-pAzF was a gift from Dr. Peter Schultz (Addgene; plasmid 31186).

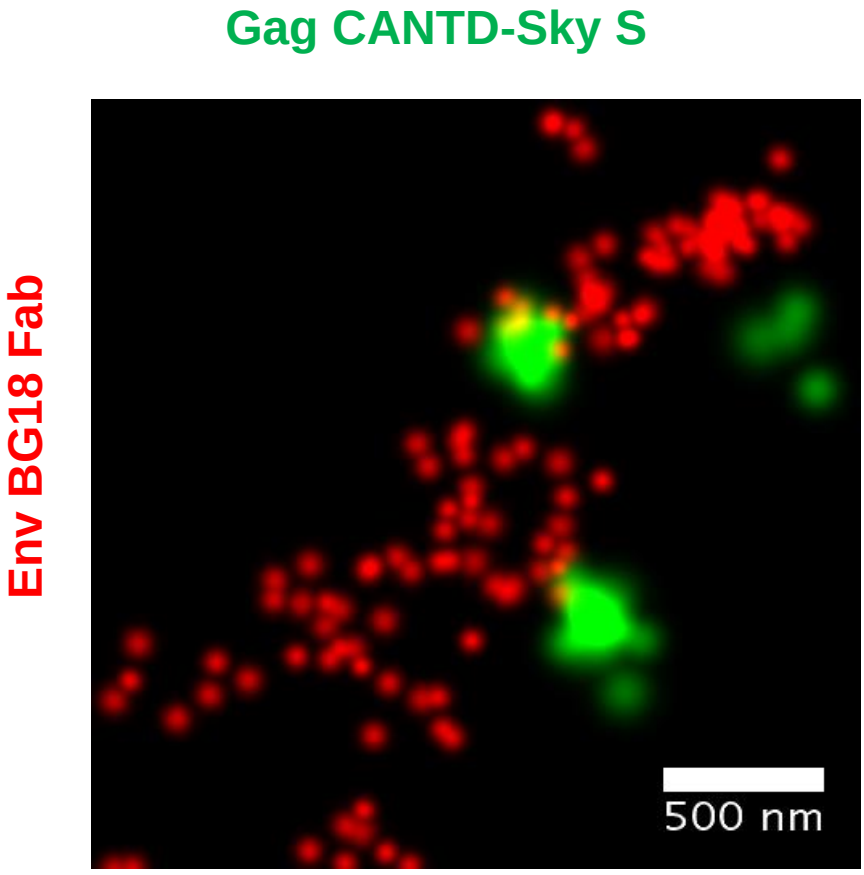

Figure 2.2. TIRF imaging of BG18-QD625 labeling Env-ΔCT trimers, and Gag CANTD-SkylanS nanobody expressed in live COS7 cells

Multiple Env-ΔCT trimers (red) demonstrate mobile Env nature at Gag labeled HIV-1 assembly sites with CANTD-SkylanS nanobody (green). The high labeling density of BG18-QD625 achieved, allows for improved quantification of Env single particle tracking during assembly events. Normalized and rendered to Gaussian peaks, width correspondence to uncertainty in position. Scale bars, 500 mm.

Chapter 3

A Quantitative Live-Cell Superresolution Imaging Framework for Measuring the Mobility of Single Molecules at Sites of Virus Assembly

Abstract

The insurgence of superresolution microscopy into the fields of virology and microbiology has begun to enable the mapping of molecular assemblies critical for host–pathogen interfaces that organize on a scale below the resolution limit of the light microscope. It is, however, challenging to completely understand the molecular interactions between host and pathogen from strictly time-invariant observations. Herein, we describe a method using simultaneous dual-color superresolution microscopy to gain both structural and dynamic information about HIV-1 assembly. Specifically, we demonstrate the reconstruction of single virus assembly sites using live-cell photo-activated localization microscopy (PALM) while concurrently assessing the sub-viral mobility of the HIV-1 envelope glycoprotein during interaction with the viral lattice. We propose that our method is broadly applicable to elucidating pathogen and host protein–protein interactions through quantification of the dynamics of these proteins at the nanoscale.

Introduction

Since its inception, superresolution microscopy has been broadly adapted to many fields of biological study (Betzig *et al*., 2006; Hell, 2007; Rust *et al* 2006; Hess *et al*., 2006; Schermelleh *et al*., 2008). Such methods offer molecular specificity and resolution improvements up to 10-fold over conventional diffraction-limited microscopy, enabling the reconstruction of biological assemblies approaching tens of nanometers (Buttler *et al*., 2018). With these tools in hand,

researchers have been able to assess cellular spatial organization of molecular assemblies created by pathogens, enabling the nanoscale visualization of host–pathogen interfaces (Zhang *et al*., 2017; Han *et al*., 2014; Liu *et al*., 2018; Gray *et al*., 2016; Horsington *et al*., 2013; Hess *et al*., 2007; Laine *et al*., 2015; Floderer *et al*., 2018). In particular, superresolution imaging has provided powerful insight into the mechanisms of human immunodeficiency virus-1 (HIV-1) particle biogenesis and maturation (Buttler *et al*., 2018; Lehmann *et al*., 2011; Chojnacki *et al*., 2012; Pereira *et al*., 2012; Gunzenhäuser *et al*., 2012 Roy *et al*., 2013 Muranyi *et al*., 2013; Van Engelenburg *et al*., 2014 Hendrix *et al*., 2015 Boutant *et al*., 2020 Fogarty *et al*., 2014). While these studies have been powerful for uncovering new aspects of protein organization during HIV-1 biogenesis, this methodology has been largely relegated to time-independent measurements and lacks spatiotemporal information regarding viral protein coalescence. These shortcomings have been addressed using fluorescence recovery after photobleaching (FRAP) to measure bulk diffusion rates for viral molecules, however, this technique cannot provide resolution below the the diffraction-limit (Sakin *et al*., 2017). Stimulated emission depletion microscopy in conjunction with scanning fluorescence correlation spectroscopy (STED-FCS) presents a route to measure diffusion rates of viral molecules below the resolution limit of the light microscope (Chojnacki *et al*., 2017). In addition, single particle tracking (SPT) is an orthogonal and readily accessible method that can provide spatiotemporal information of single viral molecule dynamics on the scale of one to tens of nanometers (Pezeshkian *et al*., 2019). Combinations of both STED and SPT have also been demonstrated (Inavalli *et al*., 2019).

Upon infection, HIV-1 Gag oligomerizes on the inner leaflet of the plasma membrane in T-cells by a cooperative interaction between its N-terminal membrane-binding domain and internal Capsid (CA) oligomerization domain(Saad *et al*., 2006; Alfadhli *et al*., 2009; Ono *et al*., 2004; Li *et al*., 2000; Gamble *et al*., 1997). After reaching a critical mass of oligomers, the forming lattice will buckle the plasma membrane to create a virus bud (Jouvenet *et al*., 2008; Ivanchenko *et al*., 2009). To form an infectious particle, the HIV-1 envelope glycoprotein (Env) must traffic from the

biosynthetic pathway to reach the plasma membrane. Upon reaching the plasma membrane, Env freely diffuses and either becomes trapped in a newly formed Gag lattice or is endocytosed (Checkley *et al*., 2011; Byland *et al*., 2007). Previously, we described the spatiotemporal dynamics of HIV-1 Env on a sub-viral scale (tens of nanometers) during HIV-1 biogenesis on living cells (Pezeshkian *et al*., 2019). Our SPT method allowed for simultaneous measurement of heterogeneous diffusion modalities and trapping of Env at sites of Gag lattice formation, which was dependent upon residues in both Gag and Env. Our previous approach relied on conservative estimates of Env proximity to Gag lattices due to diffraction-limited resolution of virus assembly sites, creating uncertainty in the location of the perimeter of these assembly sites. For strong phenotypic differences this uncertainty becomes negligible, however, this error becomes significant as genetic phenotypes become more nuanced. Herein, we expand on our previous methodology by providing a framework for measuring live-cell nanoscale dynamics using superresolution photo-activated localization microscopy (PALM) of the Gag lattice paired with single particle tracking of HIV-1 Env. Although we have focused this methodology on HIV-1 assembly, this method is broadly applicable to other virus species and microbial receptor interactions.

Results

2.1. Simultaneous Superresolution Reconstruction and Tracking of HIV-1 Gag and Env

To track HIV-1 Env with respect to sites of virus assembly on the plasma membrane of living cells, we used total internal reflection fluorescence microscopy (TIRF-M) with simultaneous dual-wavelength monitoring. To reconstruct sites of Gag assembly below the diffraction-limit of the light microscope, we used a genetically encoded Camelid antibody (nanobody), targeting the Capsid (CA) domain of Gag, fused to the photoswitchable fluorescent protein Skylan-S (Helma *et al*., 2012; Zhang *et al.,* 2015), and expressed from the viral genome. Previously, we demonstrated that the CA nanobody has no known perturbing effects on the formation of virus

particles (Pezeshkian *et al*., 2019). We screened several green photoswtichable fluorescent protein variants from the Skylan series and selected Skylan-S (mEOS3.1 parent with H62S mutation) as it displayed ideal photoswitching rates and photon output for our desired frame rate. Unlike mEOS3.1, Skylan-S does not undergo photoconversion from a green to red form (Zhang *et al*., 2015), instead it transitions between ‘on’ and ‘off’ green fluorescent states (Figure 6A).

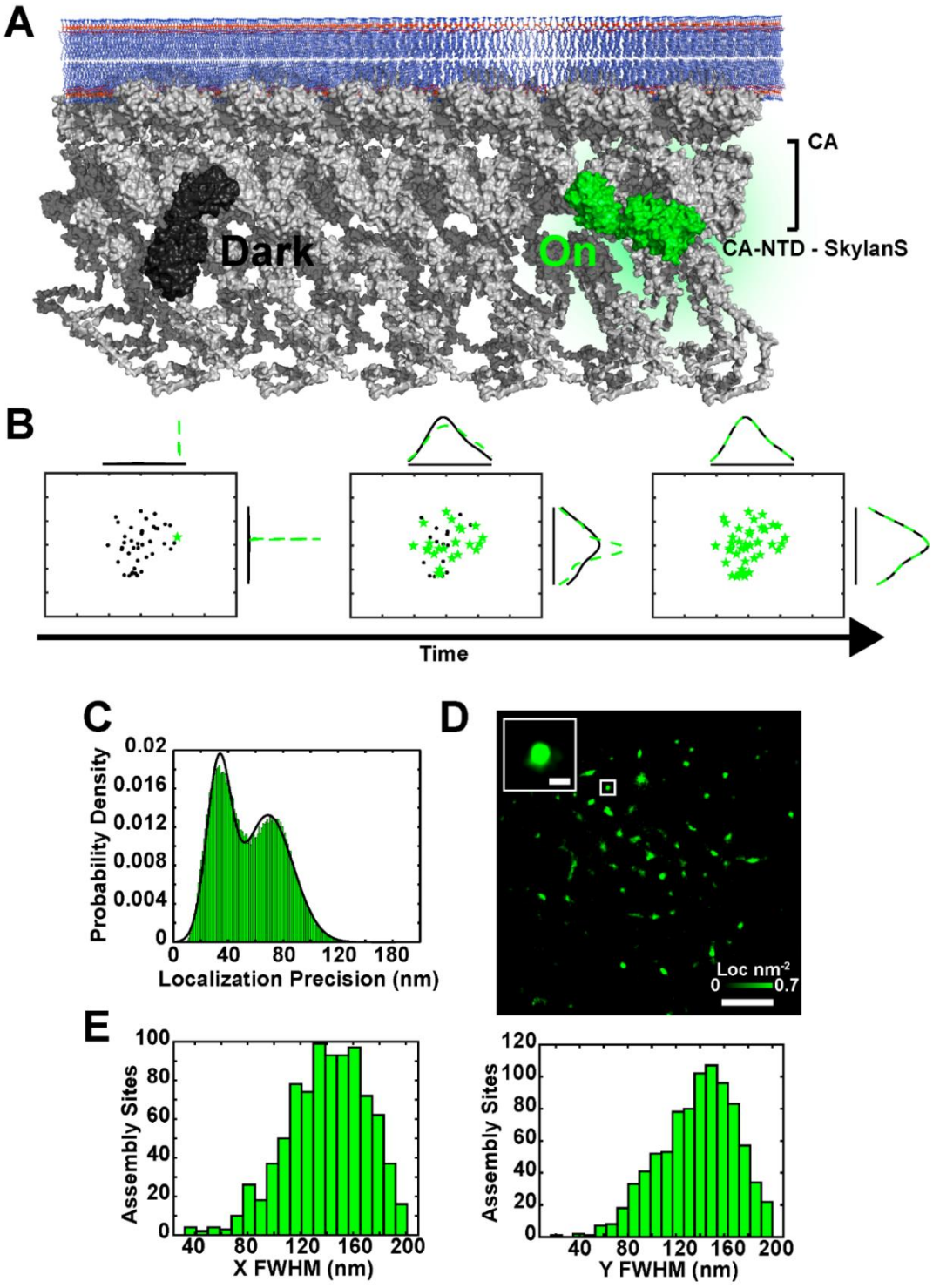

Figure 3.1. CA-Skylan-S probes accurately reconstruct HIV-1 assembly sites on live infected T-**cells.** (**A**) The HIV-1 Gag lattice (Gray) oligomerizes on the inner leaflet of the plasma membrane (Blue). The genetically encoded anti-CA nanobody fused to Skylan-S (CA-Skylan-

S) binds specifically to the N-terminal domain of Capsid. Skylan-S undergoes photoswitching upon illumination with blue (473–488 nm) laser light, moving single Skylan-S molecules between a ‘Dark’ and ‘On’ fluorescent state (black and green, respectively). (**B**) Example of localization accumulations for a single diffraction-limited virus assembly site on a live infected CEM-A cell expressing CA-Skylan-S probes. Green represents ‘On’ molecular localizations accumulated over time. Black represents the final accumulation of localizations for the reconstructed virus assembly site. Curves are the respective probability densities in horizontal and vertical directions (X,Y) for the superresolution reconstruction showing a Gaussian-like distribution after sufficient sampling of lattice-associated CA-Skylan-S probes. (**C**) Aggregate of all uncertainties in position for each localization in all data sets is demonstrated (σ). The histogram was fit to a bimodal Gaussian probability density ($\mu\sigma_{low}$=32.9±8.9,$\mu\sigma_{high}$=68.9±18.2 nm). The larger peak was eliminated by filtering localizations to σ<40 nm and likely represents localization events in areas of high cellular background. (**D**) Assembly sites on the surface of live CEM-A T-cells were reconstructed using the localization centroids with their respective uncertainties (scale: Image = 5 μm, Inset = 200 nm. Maximum localization density: 0.7 localizations per nm2). (**E**) Full-width at half-maximum (FWHM) for segmented virus assembly sites (normal distribution fit: $\mu XFWHM$=139.8±30.5 nm; $\mu YFWHM$=137.7±31.3 nm; fit not shown). FWHM in both coordinates converge on the theoretical size of HIV-1 particles, demonstrating the ability of CA-Skylan-S probes to superresolve sites of virus assembly on living infected T-cells.

Specifically, these single fluorescence events are captured during high-speed streaming and can be subsequently fit to a Gaussian function to determine the position of the fluorescent probe. This centroid and the number of integrated photons are used to determine the uncertainty in the position measurement (Betzig *et al*., 2006) (Figure 6B,C). The accumulation of these points and their uncertainties in time enables the reconstruction of the Gag lattice below the diffraction-limit using the live-cell PALM method (Shroff *et al*., 2008) (Figure 6D). To determine whether assembly sites were reconstructed to the approximate size of an HIV-1 particle in 2-D cartesian coordinates, they were fit to a normal distribution and full-width at half maximum (FWHM) was calculated. The approximate size of the HIV-1 virus particle is ≈145 nm (Briggs *et al*., 2003), which validates 138 ± 31 nm as our mean FWHM of assembly sites (Figure 6E). We found that membrane movement and microscope drift were negligible during rapid acquisition (100 frames per second (fps); 30 s interval) as FWHM reconstructions between x and y dimensions varied by 5.8 nm (4%) for each assembly site measured. Importantly, simulations of our experimental system suggest that our FWHM reconstructions of virus assembly sites results from the localization of more than one CA-Skylan-S molecule.

To visualize single Env trimers diffusing proximal and incorporating into Gag assembly sites, we labeled Env trimers with a modified anti-Env antibody fragment (fab) conjugated to a quantum dot. The anti-Env fab, BG18, has nanomolar affinity for the glycan-V3 region of the gp120 ectodomain of Env (Freund *et al*., 2017). The fab was produced recombinantly in bacteria in order to incorporate an unnatural amino acid, p-azido-L-phenylalanine, capable of reacting site-specifically to a dibenzocyclooctynol (DIBO)-modified quantum dot via copper-free click chemistry (Pezeshkian *et al*., 2019) (Figure 7 and Figure 8A).

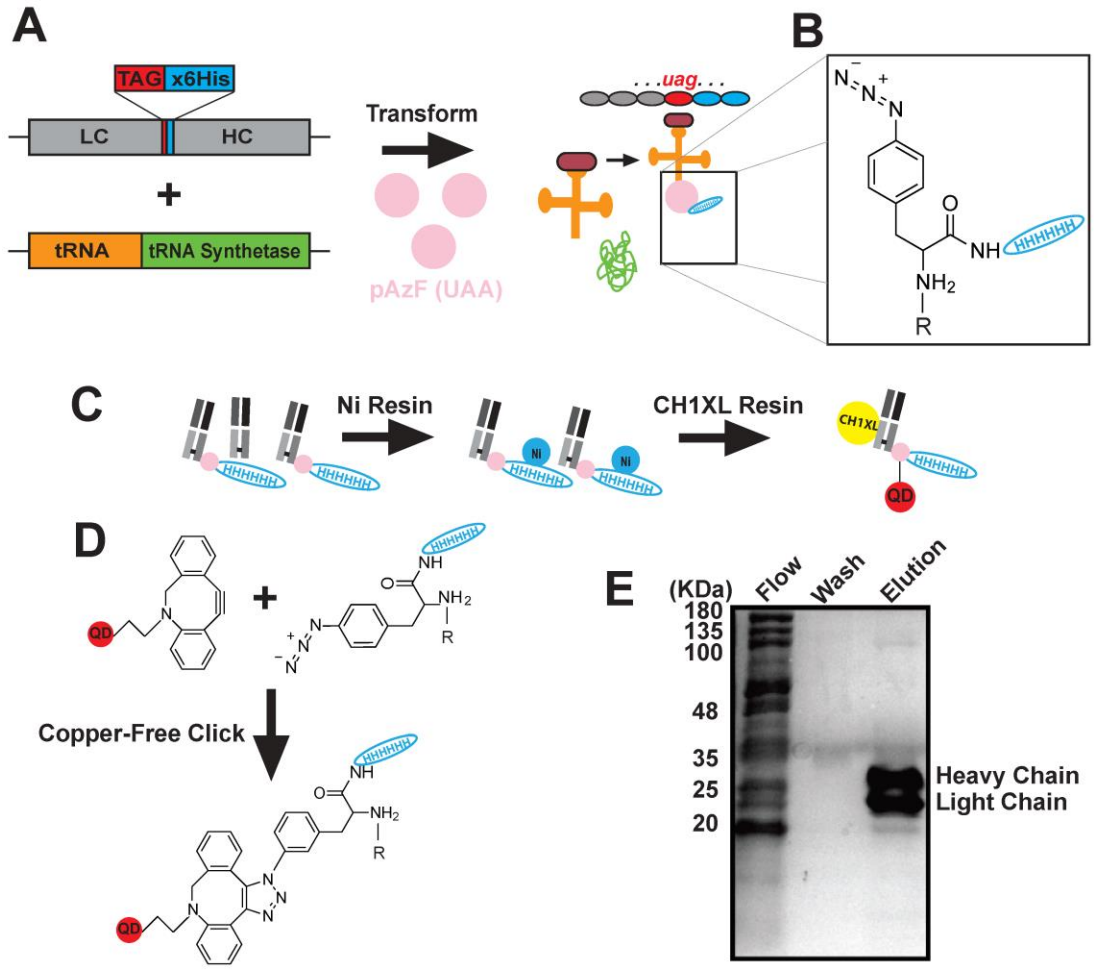

Figure 3.2. BG18-QD625 design and production

Recombinant bacterial expression system for production of BG18 containing an unnatural amino acid (UAA). E. Coli strains selected for both pCOMB3H-BG18-Amber fab and H-4-azido-phenylalanine(pAzF) tRNA/ tRNA-synthetase expression plasmids produce UAA-incorporated light chain BG18 upon pAzF-charged tRNA anticodon (AC) recognition of the Amber stop codon. (**B**) The incorporation of the UAA allows for noncanonical expression of p-azido-L-phenylalanine thereby, providing a site for a quantum dot click reaction as well as a His-(×6) tag for purification of UAA-incorporated fab (R = BG18 fab). (**C**) Cartoon protocol for the purification of BG18-QD625: (1) Metal-ion affinity chromatography of Amber-suppressed BG18 fab possessing a hexahistidine repeat after the pAzF UAA, (2) purified BG18-pAzF fab is then conjugated to DIBO-QD625 using copper-free click chemistry, (3) unreacted DIBO-QD625 is subsequently removed from BG18 fab by affinity chromatography using anti-human IgG CH1-domain resin, (4) unlabelled BG18-pAzF fab is then removed from the BG18-QD625 conjugates using a 100 kDa molecular-weight cutoff filter. (**D**) Molecular cartoon of the BG18-QD625 conjugation strategy using the copper-free click chemistry reaction. The covalent coupling reaction occurs between the strained alkyne group and the azide moiety. (**E**) SDS-PAGE of flowthrough, wash, and elution fractions after BG18 purification from both metal-ion and CH1XL affinity chromatography. Heavy and light chains

of fab complexes are purified to near homogeneity in stoichiometric abundance as assessed by Coomassie R-250 staining.

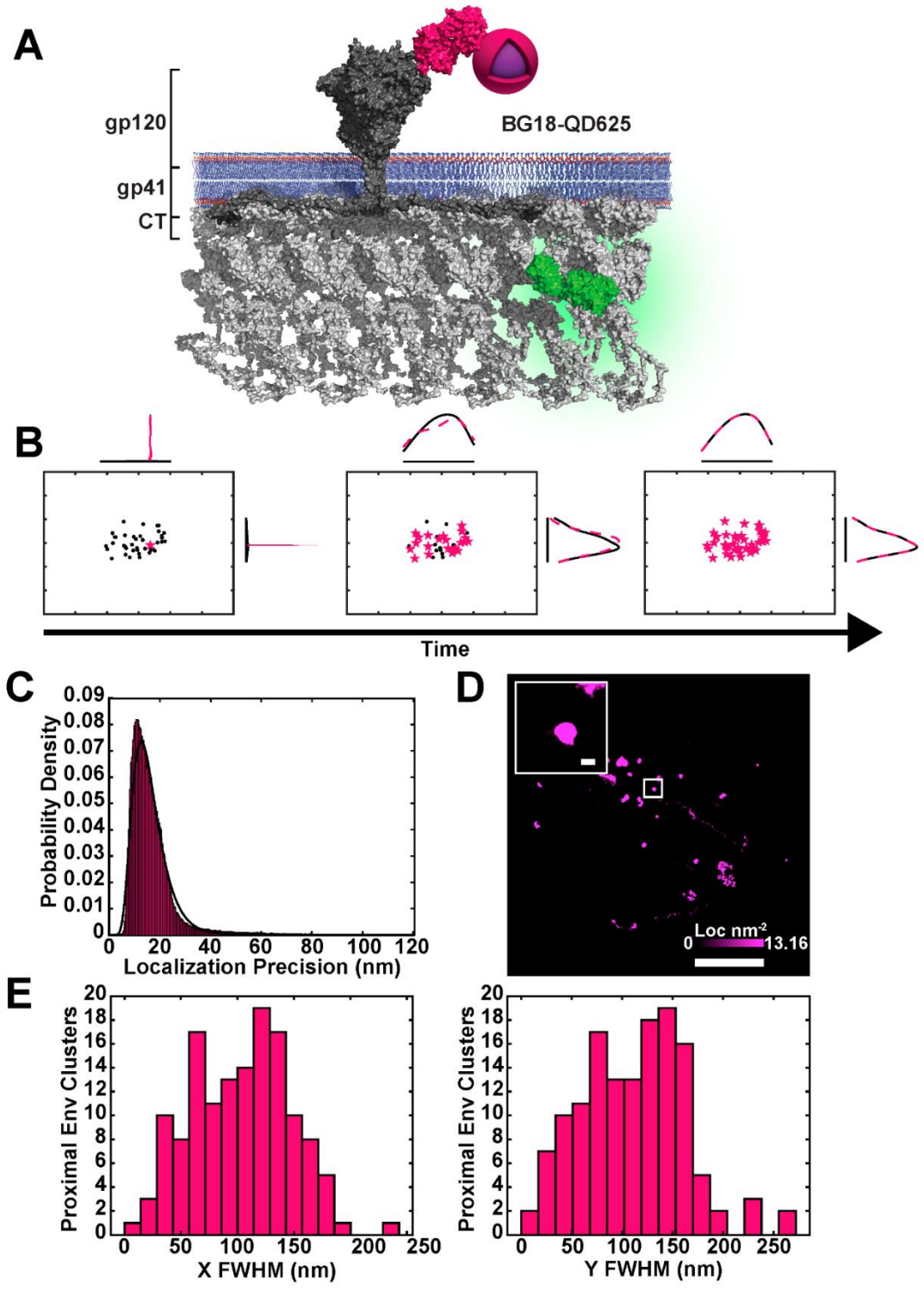

Figure 3.3. BG18-QD625 is a highly specific monovalent probe for high-density localization of single HIV-1 Env trimers.

(A) HIV-1 Env diffuses freely on the plasma membrane until encountering a Gag lattice. BG18-QD625 (Magenta) binds to a glycopeptide (V3) on the HIV-1 Env gp120 ectodomain. The gp120 domain non-covalently associates with the ectodomain of gp41, which is anchored to the membrane through the transmembrane and Cytoplasmic Tail (CT) domains, with the CT putatively interacting with or sterically trapped by the Gag lattice. (B) Temporal point localization of a single Env trimer reconstructs a diffusion trajectory. Magenta stars represent new localizations of a single BG18-QD625 probe per frame. Black represents the entire accumulation of localizations over the time of acquisition. Curves represent the probability densities in horizontal and vertical (X,Y) dimensions for sub-diffraction limited distributions of mobile trimers labeled by BG18-QD625. (C) The localization precision of BG18-QD625 labeled Env trimers is σ=16.1±6.6 nm, equating to roughly 10% of the diameter of a single virus particle, allowing for mobility measurements at a sub-viral scale. (D) Tracking of single Env trimers on living cells demonstrates that Env has a range of mobility distributions. The maximum density of localizations is 13.2 localizations per nm2 (magenta color bar) over 30 s of sampling. Inset shows a highly confined Env trimer displaying an apparent normal distribution of displacements (inset scale bar is 200 nm; full image scale bar is 5 μm). (E) Single molecule trajectories of Env classified as proximal to sites of assembly were fit to a normal curve and the FWHM was calculated (fits not shown). These tracks proved to be highly confined at the sub-viral level (μXFWHM=103.3±43.2nm and μYFWHM=111.0±52.2 nm). Clusters of Env localizations were found to be 30% smaller than the average size of virus assembly sites. This suggests that Env may be relegated to a sub-region of the viral lattice.

Conjugation of the fab to Quantum Dot 625 (QD625) provided a mean localization precision of 16.1 ± 6.6 nm at 100 fps when bound to surface exposed Env (Figure 8C). With high spatiotemporal resolution and sparse cellular labeling of Env using the BG18-QD625 probe, we were able to visualize and quantify sub-viral confinement of Env within single reconstructed Gag lattices (Figure 6D and Figure 8 B). No significant cross-talk between the two fluorescent channels was observed and QD625 fluorescence intensity remained relatively stable during imaging intervals. Env in proximity to Gag centroids were fit to a normal distribution to assess the FWHM of confinement. The mean FWHM of Env positional measurements within the viral lattice was 101 ± 48 nm, corresponding to 73 percent of the average size of viral assembly sites measured by live-cell PALM (Figure 8E).

2.2. Sub-Viral Quantification of Env Diffusion

With our results suggesting that single Env trimers in proximity to the Gag lattice have some sub-viral mobility, we then sought to quantify the differences in mobility between Gag lattice proximal and distal Env trimers. Trimers were deemed proximal to a Gag lattice if they were found within a radius of influence (ROI) measured from the centroid of the Gag lattice by the following equation:

$$ROI = \frac{\sqrt{FWHM_X^2 + FWHM_Y^2} + 2\sigma_{FWHM} + \sigma_{Registration}}{2} \quad (1)$$

where FWHM-X/-Y are the virus assembly site dimensions, σ FWHM is the standard deviation of the FWHM distribution, and σ registration is the error in alignment of the Env and Gag fluorescent channels. In regions void of a Gag lattice ROI, Env tracks were classified to be distal. We quantified the differences in mobility between proximal and distal single Env trimers by first linking Env localizations based on proximity to one another and their frame interval (see Materials and Methods for track linking description). We observed marked differences in track appearance and shape between proximal and distal tracks, with distal tracks displaying random-walk or Brownian-like motion (Figure 9a).

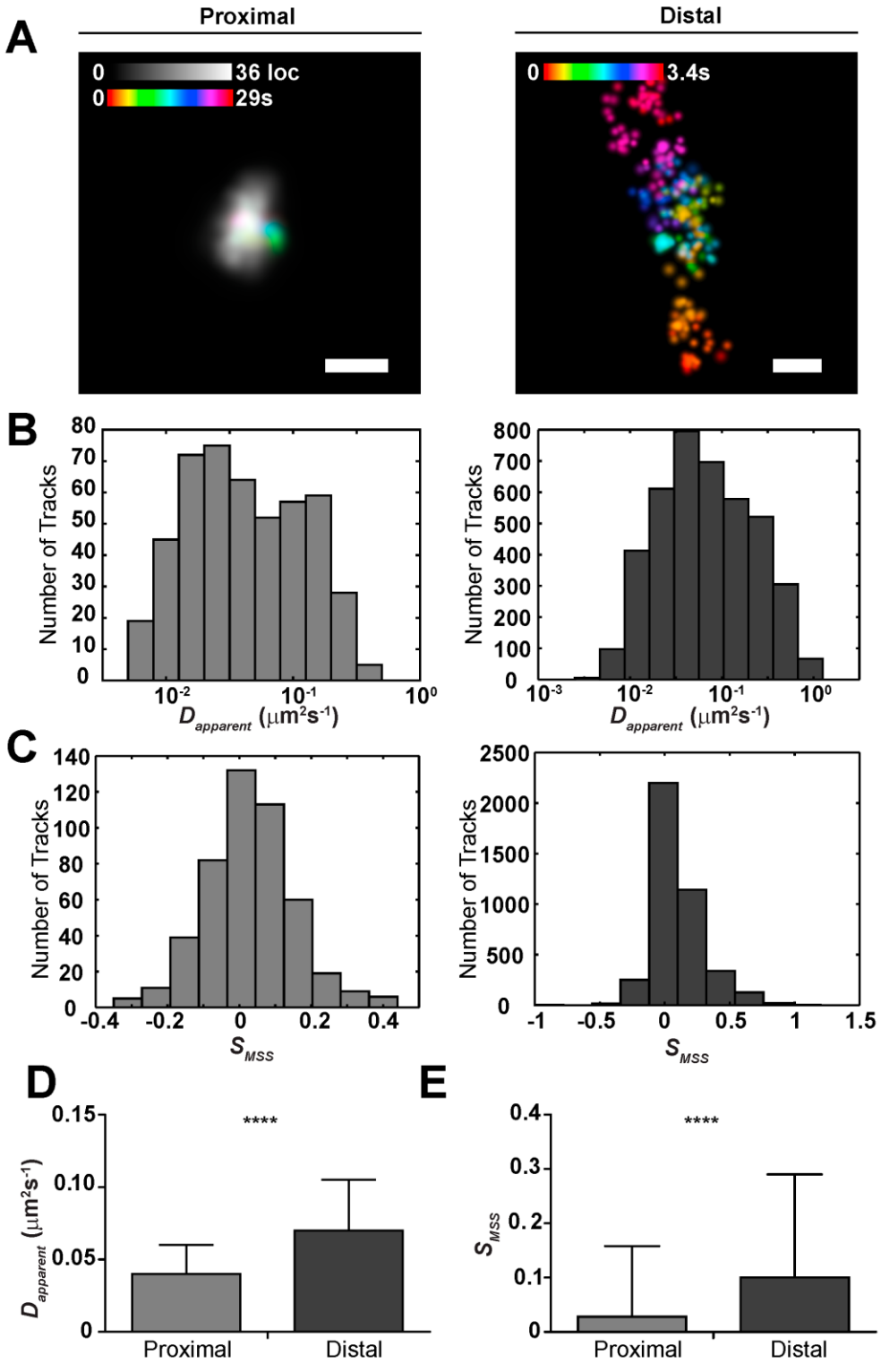
A
Proximal
Distal
0
36 loc
0
29s
0
3.4s
B
Number of Tracks
$D_{apparent}$ ($\mu m^2 s^{-1}$)
C
Number of Tracks
S_{MSS}
D
$D_{apparent}$ ($\mu m^2 s^{-1}$)
****
Proximal
Distal
E
S_{MSS}
****
Proximal
Distal

Figure 3.4. HIV-1 Env is highly confined at sites of assembly and diffuses freely when non-proximal to the Gag lattice on the surface of infected CEM-A T-cells.

(A) Representative examples of Env diffusion ‘Proximal’ and ‘Distal’ to sites of assembly (scale bars are 200 nm; Env: time-colored gradient; Gag: gray localization density). When proximal, Env was never observed to escape the Gag lattice over the sampling period, yet is able to freely diffuse when distal to assembly sites. Width of points represent uncertainty in localization of a single molecule in the time-series. (B) Histograms of the apparent diffusion coefficient (Dapparent) for proximal and distal tracks in log10 scale (Dapparent=0.04±0.02 μm2× s−1 and 0.07±0.04 μm2×s−1, respectively). (C) Histograms of the slope of the moment scaling spectrum (SMSS) for proximal and distal tracks (SMSS=0.03±0.13 and 0.10±0.02, respectively). (D,E) Dapparent and SMSS for proximal versus distal trajectories were found to be statistically significant with a respective increase in both parameters for distal trajectories suggesting that Env trimers are less mobile and more sub-diffusive when proximal to a Gag lattice. Significance was assessed using a two-tailed unpaired t-test (PDapparent=2.67×10−17; PSMSS=1.04×10−15; α=0.0001; NProximal=476, NDistal=4089). Error bars represent standard deviation.

Next, we computed the apparent diffusion coefficient (D*apparent*) and slope of the moment scaling spectrum (SMSS) for individual tracks, which mathematically describe the area covered by a single molecule in unit time and how well the molecule samples that area, respectively (Qian *et al*., 1991; Ferrari *et al*., 2001). There was a significant shift in both Dapparent and SMSS between proximal and distal tracks (PDapparent=2.67×10−17, PSMSS=1.04×10−15). D apparent for proximal tracks (0.042 μm2s−1) was roughly 40 percent lower than for distal tracks (0.068 μm2s−1), indicating that the Gag lattice acts as a net-like diffusion barrier for the Env trimers when incorporated. Apparent magnitude of a Gag bud is measured to tell how bright the assembly site appears at its distance from another separate assembly site. There was also a 70 percent reduction in SMSS for proximal (0.028) versus distal tracks (0.099). Because the SMSS parameter indicates the shape or trajectory of a track as it samples an area of the membrane, a reduction in SMSS implies a more confined trajectory.
An SMSS=0.028 and Dapparent=0.042μm2s−1 for proximal Env concludes that the tracks are highly confined, with sub-viral diffusion over the time frame of acquisition (≈30 s). Quantification of these parameters suggests that Gag has a significant influence on Env during virus assembly compared to distal Env trimers on the plasma membrane (Figure 9).

The described methodology provides greater precision in the measurement of the Gag lattice perimeter, thus reducing the misclassification of proximal versus distal tracks and the associated error in diffusion measurements. Concurrently, our optimized BG18-QD625 probe enables tuneable high-density localization and tracking of single Env trimers on the surface of infected cells with tens of nanometers of precision.

Discussion

Many aspects of virus biogenesis remain enigmatic due to our inability to resolved the time-variant structural organization of viral sub-assemblies while simultaneously maintaining molecular specificity and physiologically relevant conditions. Time-resolved superresolution approaches, however, offer promise to further our understanding of the molecular steps and sequences of events that transpire during virus assembly. In this study, we present a method for sub-viral quantification of biophysical interactions between single molecules of HIV-1 envelope glycoproteins and the structural Gag lattice using live-cell single particle tracking and superresolution microscopy, respectively. This approach has allowed us to visualize nanoscale interactions between these molecules during virus biogenesis on the host-cell plasma membrane. We have shown that Gag lattices can be reconstructed to expected virus dimensions, below the diffraction-limit of the light microscope, using live-cell PALM. Further, we show that Env trimers can be simultaneously tracked and quantified based on their precise proximity to superresolved virus assembly sites.

Our approach has relied on the use of a genetically-encoded cytoplasmically-expressed nanobody fused to a reversibly switchable fluorescent protein to reconstruct virus assembly sites. The success of live-cell PALM is highly dependent on how well the sub-diffractive object is decorated with a fluorescent probe. We show that the CA-Skylan-S nanobody probe sufficiently samples the Gag molecules in a single virus assembly site because each superresolved image over a 30 s time course yields a FWHM approximately the size of expected virus assembly sites measured by electron microscopy (Briggs *et al*., 2003). The success of live-cell PALM imaging additionally requires sufficient sampling of each fluorescent probe within the structure of interest and high molecular brightness to reduce the

uncertainty in the position of each probe. We judiciously selected the Skylan-S reversibly-switchable green fluorescent protein for its single molecule brightness and switching frequency. Skylan-S enabled us to sufficiently sample each nanobody tagged probe a few times before bleaching irreversibly, while also giving a sufficiently high photon count for each frame to more precisely localize single molecule probes. Our attempts with other variants of the Skylan series of reversibly-switchable green fluorescent proteins resulted in either low molecular brightness and poor localization precision or poor switching properties resulting in a lack of blinking and single molecule detection (data not shown). Finally, live-cell superresolution reconstructions require careful consideration of physical displacements of the object of interest, requiring tuning of sampling conditions to reduce motion blur artifacts (Shroff *et al*., 2008; Huang *et al*., 2013). In the case of HIV-1 Gag lattice formation, this structure remains sufficiently static over the sampling period (30 s) as evidenced by the FWHM reconstructions and expected diameters of HIV-1 particles.

Using our optimized fluorescent label and sampling conditions, we still, with minor frequency, found that our software filters out what is likely an assembly site that cannot be properly fit due to lack of localizations. Insufficient sampling at putative virus assembly sites, due to poor CA-Skylan-S probe labeling or sampling, may contribute to erroneous classifications of Env, resulting in an increase in apparent diffusion coefficient and SMSS distribution error. The sparsity of Env labeling with our methodology, however, statistically reduces the frequency of these false-negative events.

Additional considerations for implementation of this methodology are the production of a recombinant antibody fragment, subsequent site-specific unnatural amino acid modification and copper-free click chemistry to a quantum dot (Figure 7 and Materials and Methods). While unnatural amino acid constructs are publicly accessible and quantum dot kits are commercially available, production of the probe in usable quantities can be costly and technical for adopters without recombinant protein chemistry experience. The BG18-QD625

probe described here is a prime example of a highly optimized recombinant protein expression protocol and tuned conjugation chemistry, which yields large quantities of stable probe that can be used for months to years. Ultimately, live-cell superresolution and SPT methodology requires highly specific and high affinity (sub-10 nM dissociation constant) monovalent reagents for labeling of biological structures of interest due to the intrinsic single molecule sensitivity of these experiments.

The optimization of the CA-Skylan-S probe has provided a means for precise superresolution reconstructions of single HIV-1 assembly sites on the surface of live infected T-cells. Importantly, this resolution improvement has the potential to measure minor perturbations to Env mobility during lattice trapping. Further, our optimized production and validation of the BG18-QD625 probe has enabled us to tune the density of labeled Env trimers to maximize data collection on a per cell basis. This methodological advancement has provided insight into the biophysical interactions between the critical vaccine target HIV-1 Env and the underlying Gag lattice that coalesce to create an infectious virus particle. The sub-diffusive nature of Env in the Gag lattice could indicate a direct interaction between the membrane proximal matrix (MA) domain of Gag and the cytoplasmic tail of Env (Env-CT). We cannot rule out a physical or steric corralling mechanism, however, which creates a diffusion barrier to trap Env in a sub-diffusive state within the lattice. Further work will be aimed at elucidating potential molecular interactions using the methodology we have presented. Studies investigating diffusional behaviours of viral envelope glycoproteins with their respective structural components should lead to discovery of new therapeutic approaches that target virus assembly.

Materials and Methods

4.1. Reagents

The HEK293T (CRL-3216) cell lines were obtained from ATCC (Manassas, VA, USA). The CEM-A cell line was obtained through the NIH AIDS Reagent Program, Division of AIDS, NIAID, NIH: CEM-A from Dr. Mark Wainberg and Dr. James McMahon, CEM-CL10 (Tremblay *et al*., 1989). Cell lines were grown at 37 ∘C with 5% CO_2. Complete growth medium for HEK293T cells was prepared by combining 10% fetal bovine serum (Corning; Corning, NY, USA), 2 mM L-glutamine (Corning), and Penicillin-Streptomycin (Corning) into Dulbecco's Modified Eagle's Medium (DMEM) (Corning) or for the CEM-A cell line with identical ingredients into Roswell Park Memorial Institute (RPMI) medium (Corning). Additionally, the CEM-A cell line growth medium was supplemented with 1% hypoxanthine, thymidine (HT) solution (Corning).

4.2. Generation of CA-Skylan-S Expressing Viruses

The pSV-NL4-3 reference HIV-1 genome was used for all experiments with constructs possessing deletions in the gag-p6 late-domain, *pol*, *vif*, *vpr*, and *nef* genes (Buttler *et al*., 2018). To create viral vectors coexpressing the CA-Skylan-S nanobody, the coding region for the anti-CA nanobody was genetically fused to the Skylan-S gene with a coding amino acid linker of: 'RSFEFCSRRYRGPGIHRPVAT'. The CA-Skylan-S probe cassette was amplified with 5′ and 3′ Gibson homology arms against the coding regions of the 3′ end of *env* and 5′ end of the *nef* coding regions, respectively. Replication incompetent viruses harboring the CA-Skylan-S nanobody cassette in the *nef* splice site were produced by transfecting HEK293T cells with pSV-NL4-3 (described aboe) vector, pSPAX2 (Addgene, plasmid #12260), and pVSV-G (Addgene, plasmid #8454). Supernatants from cells expressing for 48 h were stored at −80 ∘C prior to infection.

4.3. Monovalent BG18-QD625 Production

The BG18 anti-Env V3 glycan-binding light and heavy chain antibody sequences were obtained from the Protein Data Bank (6CH9) (Barnes *et al., 2018)*. The fragment of antigen binding sequences were synthesized (IDT; Coralville, IA, USA) and cloned into the pCOMB3H-b12 vector using SacI and NotI sites, replacing the b12 fab coding sequence (Barbas *et al*., 1994). The pIII region of pCOMB3H was suppressed by introduction of a stop codon at the end of the BG18 heavy chain CH1 domain. The light chain gene fragment from BG18 was engineered to contain a 3′ amber stop codon (TAG) followed by a 6-fold repeat of histidine codons, finalized with an ochre stop codon (TAA). Periplasmic expression of BG18 fab containing a C-terminal p-azido-L-phenylalanine (pAZF) unnatural amino acid (Bachem; Torrance, CA, USA) was performed in *Escherichia Coli* XL1 Blue competent cells (Stratagene; San Diego, CA, USA) by co-transformation with pCOMB3H-BG18-LC-Amber-His6-Ochre and pEVOL-pAzF. Briefly, this strain was grown in 1–2 L of Super Broth medium containing selective antibiotics. At mid-log phase, 1 mM unnatural amino acid pAZF was added to the culture and expression of unnatural tRNAs and synthetase was induced with 2% (w/v) L-arabinose (Gold Biotechnology; St. Louis, MO, USA). Cellular lysates were produced by sonication in PBS pH 7.4 supplemented with 0.2 mM PMSF (Gold Biotechnology). Soluble proteins were clarified via centrifugation at 30,000× *g* for 30 min and filtration by 0.22 μm cellulose acetate syringe filter. BG18 fab that successfully suppressed the amber stop codon with pAZF was purified using Nickel affinity chromatography (Gold Biotechnology) followed by purification using CaptureSelect CH1-XL affinity chromatography resin (Thermo Scientific; Waltham, MA, USA). Elution fractions were pooled and dialyzed overnight in PBS, pH 7.4. Expression was assessed (Figure7F) by SDS-PAGE analysis on 4–20% gradient gel (Bio-Rad; Hercules, CA, USA). The final yields from 1–2 L of culture were typically in the range of 1–3 mg of BG18-pAzF.

Copper-free click chemistry was performed between DIBO-QD625 (Site-Click kit, Thermo Scientific) and BG18-pAzF using a 1:1.5-fold stoichiometry, respectively. The reaction was allowed to proceed for 12–18 h at room temperature in the dark. Uncoupled DIBO-QD625 was removed from the reaction by another round of CaptureSelect CH1-XL affinity chromatography. Elution fractions were pooled and unreacted BG18-pAzF, lacking a DIBO-QD625 conjugate, was removed by filtration through a 100 KDa molecular weight cutoff filter (Site-Click kit) followed by repeated buffer exchanges with PBS, pH 7.4.

4.4. Sample Preparation and Imaging Conditions

CEM-A T-cells in complete RPMI medium were dispensed onto 25 mm No. 1.0 glass coverslips (Warner Instruments; Hamden, CT, USA) at high density and allowed to adhere for 18–24 h at 37 ∘C and 5% CO_2. Cells were infected with replication-incompetent (single-round infection) virus and incubated for 38–46 h prior to imaging. Coverslips were transferred to specimen holders and mounted on a custom-built ring-TIRF microscope with an environmental chamber maintaining 37 ∘C and 5% CO_2 previously described (Pezeshkian *et al*., 2019). Briefly, BG18-QD625 and CA-Skylan-S probes were both excited with 473 nm laser light (50 mW at rear aperture) and fluorescence was detected by separating the respective wavelengths with a dichroic beamsplitter and W-View Gemini image splitter (Hamamatsu, Hamamatsu City, Japan). Images of each channel were then focused onto two halves of a liquid cooled ORCA Fusion scientific-CMOS camera (C14440-20UP). Images were streamed at 100 Hz.

4.5. Image Processing and Analysis

All imaging, single molecule localization, and channel registration was done per Pezeshkian et. al., 2019 (Pezeshkian *et al*., 2019). Briefly, raw images were corrected for non-uniform pixel offset by use of a calibration map and were subsequently split based on wavelength. For CA-Skylan-S, frames with 10 ms exposure were integrated to 50 ms before

single molecule localization and fitting using custom software (IDL, Harris Geospatial; Broomfield, CO, USA). A high density map of bead localizations using TetraSpeck fiducials (Thermo Fisher Scientific) was used to create a polywarp transform using the cp2tform function in Matlab (Mathworks, Natick, MA, USA) to correct for lateral chromatic aberration between the channels. Single molecule localizations were then handed to an automated package written in MATLAB. CA-Skylan-S localizations with precision below 40 nm were used to reconstruct a 50 nm pixel size binned image. This image was sent through a cluster finding algorithm which extracted each Gag cluster centroid (window 150 × 150 nm) using a threshold that requires a minimum number of localizations and integrated probability density above 1 standard deviation from the background. Single molecule localizations of Env were then deemed proximal or distal to a Gag lattice by use of Equation (1). The separated localizations were then linked using a previously described track linking algorithm adapted to MATLAB from Crocker and Grier 1996 (Crocker *et al*., 1996). The parameters for linking are as follows: 50 ms time gap, 10 minimum localizations per track, 1 pixel (108.33 nm) maximum frame to frame distance. The remaining tracks were analyzed as previously described by using the moment scaling spectrum to calculate Dapparent and SMSS (Pezeshkian *et al*., 2019; Ferrari *et al*., 2001). Mean squared displacement (MSD) was fit to a linear regression solving for Dapparent using the lag time, τ (Equation (2)).

$$MSD = 4D_{apparent}\tau^{\alpha} \quad (2)$$

Localization uncertainties were then used to weight the MSD fits (Equation (**3**)), where Ro is displacement and σR is standard deviation.

$$\frac{\Sigma \sigma_R R^o}{\Sigma(\sigma_R)} \quad (3)$$

4.6. Monte Carlo Simulations of Single Molecule Localization and HIV-1 Assembly Site Reconstruction

Simulations were performed using custom scripts written in MATLAB. Simulations were designed to assess the accuracy of reconstructions and centroid finding for scenarios with differing numbers of CA-Skylan-S probes per lattice and variances in molecular reappearance. CA-Skylan-S molecules were semi-randomly distributed on the surface of a sphere with a radius of 75 nm. Our simulations constrained the molecular positions to discontinuous regions between the polar angles (5π3,π3) and (2π3,4π3) to mimic the open neck of the viral bud and the increased accessibility of equatorial CA binding sites, respectively. True molecular positions were then shifted pseudo-randomly to mimic centroid uncertainty. This pseudo-random displacement vector was selected from a normal distribution centered around its position with a standard deviation of 50 nm, approximately the sum of our maximum localization uncertainty and standard deviation of our localization precision in experimental data (σmax=40±9 nm). Each simulation used a fixed number of molecular reappearances (α= 1 to 5) resulting in total localizations (1 to 50) to assess the accuracy of reconstruction. For each condition, 50 simulated assembly site X/Y-FWHM and centroids were averaged for each value of α.

Chapter 4

anti-HA ScFv-QD625

Introduction to Serinc5

The serine incorporator protein 5 commonly known as, SERINC5 (SER5), is a host viral restriction factor that weakens HIV-1 infectivity by incorporating in newly formed virions and inhibiting Env mediated fusion with target cells (Sood et al., 2017). The mode of action of SER 5 is currently unclear, however it has been confirmed that the MOA is related to Env inactivation and involves fusion events. SER 5 modifies the Env structure thereby exposing the virus to bNabs targeting immunogenic Env epitopes (Sood *et al*., 2017). SER 5 also has been shown to quicken the loss of Env function over time (Chen *et al*., 2020). Env clusters have been found on the surface of mature virions in many studies and SER 5 has also been shown to form clusters on the plasma membrane surface of single virions (Zhu *et al*., 2003; Buttler *et al*., 2018; Chen *et al*., 2020). The incorporation of SER 5 perturbs Env clusters but does not downregulate the Env content thereby, explaining the likely mode of action of SER 5-mediated restriction of fusion (Chen *et al*., 2020). The Sood et al. group was able to demonstrate via fusion assays, the various impairments of fusion based on the Env genotype. The effect of SER 5 on HIV-cell fusion was tested by comparing the fusion activity of different pseudoviruses that contained and excluded SER 5 in their membrane and used inactive SER 2 as a negative control. As expected, results showed incorporated SER 5 had a significantly higher inhibitory effect on HIV-1 fusion as SER 2 did not via a viral fusion assay.

Measuring viral fusion in identical assays, it was shown that the cytoplasmic tail on gp41 of Env, has no effect on inhibition in correlation with SER 5. With full expression of SER 5, a truncated Env cytoplasmic trimer tail, Δ CT, has shown significantly fewer fusion events than a full length Env trimer (Sood *et al*, 2017). These results explain the phenomena that is already known inregard to Env CT length and Gag interactions therefore, it is most likely the efficiency of Env incorporation into virus particles that explain the decrease in fusion events (Buttler *et al*., 2018; Bhakta, *et* al., 2011; Byland *et* al., 2007; Pezeshkian *et* al., 2019).

Finally, potential Env inactivation and fusion disruption has been shown by using pseudoviruses containing SER 5 and tested to see if impairment occurred in the ability to form syncytia. Syncytia is a fusion event that has been demonstrated by HIV particles and other enveloped viruses, and is the process involving particles fusing to target cells in the absence of viral replication. This process is also referred to as “fusion from without” (Clavel & Charneau, 1994). It was expectedly found that SER 5 containing viruses produced significantly less syncytia events compared to the SER 2 containing control viruses. SER 5 was expressed in the same ratio with Env as previous experiments mentioned above in the syncytia assays (Sood et al., 2017).

Though the antiviral mode of action of SER 5 is still to be completely understood, it has been demonstrated that there is an occurrence of SER 5-mediated restriction of fusion. Speculation has allowed for elucidation of other traits and dynamics of SER 5 and other key factors involved. The serine incorporator proteins are transmembrane proteins that pass through the membrane multiple times and are involved in serine incorporation into lipids and promotion of phosphatidylserine and sphingomyelin biosynthesis (Inuzuka, 2005). The HIV accessory protein known as Nef, is a player that can majorly impact pathogenicity as it is necessary for high virus loads and plays a role in infectivity (Usami et al., 2015). Nef’s mode of action is not completely understood either however, SER 5 has been observed to be antagonized by Nef. In a study using fluorescence microscopy and immunoprecipitation blotting the functionality effect of virion

infectivity was observed. Using Jurkat Tag cells, a cell line with high responsiveness to Nef, and SER 5 genomic knockouts it was shown that SER 5 knockout cells produced a 20–30-fold increase in the infectivity of the Nef-defective HIV-1, whereas the Nef-positive virus was only affected 2–3-fold, thus reducing the Nef effect from 50- to 3-fold (Rosa et al., 2015).

In conclusion, SER 5 recently has been characterized as an HIV-1 host restriction factor though its unique mechanism of restriction remains unclear. With the information that is known it can be concluded that in order to investigate SER 5, an extracellular probe and live cell time lapsed assembly and post-assembly assays will be essential to the discovery of the mechanism of action.

SER5 KI & HA Tag

To present day, there remains a search for antibodies with sensitivity and specificity for the investigation of SER 5. Currently, CRISPR/Cas9 gene editing development has yielded a human T-cell line, Jurkats, allowing for the endogenous expression of SER 5, with an exposed extracellular HA epitope [JurkatSERINC5(iHemagglutinin (HA) knock-in) T cells]. These SER 5 iHAknock-in cells equaled the parental Jurkat cells in their ability to produce infectious wild-type HIV-1 but not an HIV-1 Δ*nef* mutant (Passos *et al*., 2019). Using CRISPR-Cas9 as a manipulatable tool for site-specific gene editing has enabled tagging of endogenous proteins in human cells (Cong *et al*., 2013; Mali *et al*., 2013; Ratz *et al*., 2015). With a shortage of SER 5 antibodies available and an abundance of HA antibodies on the market, an HA knock-in expression increases the likelihood of finding a desirable tracking probe for SER 5. The extracellular HA epitope serves as an ideal target for a molecular fluorescently labeled probe to investigate SER 5 and its role in HIV-1 restriction, as an intracellular probe.

Hemagglutinin (HA) is the major surface envelope glycoprotein of an influenza virion, and its mechanism of action serves as virus entry into the host cell to initiate infection (Smith *et al*., 2004). The HA tag is a short peptide consisting of 9 amino acids which correspond to residues

98-106 of the human influenza HA molecule (Zhao, 2015). The HA tag is popularly used as an epitope tag in expression vectors and allows for the detection, isolation, and purification of proteins as there are many commercial monoclonal and polyclonal HA antibodies available for purchase. It also has been shown that recombinant proteins are commonly cloned with the HA epitope tag as it does not appear to interfere with the protein's bioactivity or function (Zhao, 2015). Overall, an HA tag serves as an ideal epitope for the protein of interest, SER 5, to allow for investigation of the mechanism of action.

In the search for therapeutic broadly neutralizing antibodies for influenza A virus strains, phage display technology was used to select single-chain variable fragments (scFv) recognizing the influenza envelope protein, HA. After several rounds of phage display, one of the HA ScFvs in trial was selected for preparative-scale production as soluble antibody by *E. coli*. It has been determined that the complementarity-determining region of the variable heavy chain (V_H-CDR2) binds the stem region of HA (Li *et al*., 2015). The development of an HA ScFv has served as a powerful tool for neutralization, detection, and tracking proteins of interest.

Overall, it was predicted that this HA ScFv would serve as an ideal candidate for fluorescently labeling and tracking SER 5. Our studies have investigated further into the mechanism of SER 5 with this monovalent fluorescently labeled HA ScFv-QD625 and Jurkat SERINC5(iHA knock-in) T cells. Single particle tracking and TIRF microscopy can be used to investigate SER 5's role in assembly and maturation to answer the following questions: Is Gag a major contributor to SER 5 incorporation? Is the diffusion and mobility of Env within the lipids of the plasma membrane affected by SER 5 due to hardening of the membrane and therefore fusion is affected as well as pore size formation? What does Env mobility look like in the presence and absence of Gag along with SER 5? Does the mechanism by which the fusion pore is affected slow down the fusion event all together? If this is the case and fusion is slowed, gp41 will remain in its "open" conformational state allowing Env to be more exposed for a longer time potentially exposing binding sites for neutralizing antibodies. To investigate Env and Gag interactions with

SER 5, immunolabeling during infection and live cell imagining will allow for the reveal of single particle tracking and protein-protein interactions.

Materials and Methods

a. Cloning of anti-HA ScFv

The pCOMB-3H-b12 plasmid (Addgene; Barbas *et al*., 1994) is digested with SacI and BglII restriction enzymes for 12 hours at 37℃ and purified using a Monarch Gel Extraction Kit (NEB). The anti-HA ScFv design can be found in the *appendix*. The DNA fragment containing anti-HA ScFv antigen binding sequences were synthesized (IDT; Coralville, IA, USA) and cloned into the pCOMB3H-b12 vector using *SacI* and *BglII* sites, replacing the b12 fab coding sequence (Barbas *et al*., 1994). The pIII region of the anti-HA ScFv Heavy and Light chain genes were amplified from a designed gBlock (IDR) with primers carrying SacI and BglII sites, containing pCOMB homology. Amplicons were ligated via Gibson reaction into the opened pCOMB vector. All sequencing was confirmed and validated through Quintara Biosciences.

b. Test Expressions

Immediately following DNA sequence validation, transformation of the pCOMB-3H-BG18 plasmid is performed in *Escherichia Coli* XL1 Blue competent cells (Stratagene; San Diego, CA, USA). This strain is plated on LB agar containing the selective antibiotic, carbenicillin, and incubated overnight for approximately 16-18 hours at 37°C. A population of bacterial colonies (n>6), is selected for and each colony is inoculated into 1 X 5 mL LB broth media containing carbenicillin (100 µg/ml), tetracycline (15 µg/ml) and dextrose (.02 M). Incubation then occurs overnight at 37°C in a shaking incubator at ~220-250 RPM. After 16-18 hours, observe cultures to ensure a moderate amount of growth and biofilm production. Measure the OD_{600} and select for the culture amongst the population that nears the OD_{600} of 0.3 A. Once the ideal culture has been determined, discard the remainder of the population. The entire 5 mLs of the overnight culture will

then be used to inoculate 2 x 50 mL Super Broth medium containing carbenicillin (100 µg/ml) and tetracycline (15 µg/ml) in a 250-mL flask for appropriate aeration and 2 x 50 mL Luria Broth medium containing carbenicillin (100 µg/ml) and tetracycline (15 µg/ml) in a 250-mL flask for appropriate aeration. To inoculate, spin 5 mL cultures at 4,000 xg for 5 minutes, pour off and discard the supernatant and vortex pellet with 1 mL of Phosphate-Buffered Saline, pH 7.4 (PBS). Repeat this PBS cell wash step 3 times. After discarding the final wash supernatant, 1 mL of LB is added to the pellet which is then vortexed thoroughly. 250 uLs of vortexed culture is then added to the 50 mLs of SB and LB broth flasks and swirled to mix evenly. Cultures are then grown at 37°C until mid-log phase of growth (OD_{600} is approximately 0.6 A) which is a timed averaged of approximately 8 h After mid-log phase has been reached, 2 of the flasks will be removed from the 37°C and placed into a 30°C shaking incubator with equivalent RPM. Cultures are then shaken and grown overnight for 16-18 h The cells are harvested by normalizing the OD_{600} to the limiting culture and then pouring the cultures into 50 mL conical tubes and spun for 20 min at 6,000 x g using a Fiberlite F13-14 x 50cy Fixed-Angle rotor in a Sorvall centrifuge (Thermo Scientific). The pellet is then washed (3 X 30 mL [1X] PBS). Store the pellet at -80°C for at minimum of 1 hour. *Note: storage time can be up to 1 year*.

Cellular lysates were produced by sonication in PBS pH 7.4 supplemented with 0.2 mM PMSF (Gold Biotechnology). Soluble proteins were clarified via centrifugation at 30,000× *g* for 30 min and filtration by 0.22 µm cellulose acetate syringe filter. Use a large probe, preferably the 300w Ultrasonic Homogenizer sonicator with the following settings: cycle 40% output power 1 minute ON and 4 minutes OFF (Vevor). Centrifugation was performed using the same Fiberlite F13-14 x 50cy Fixed-Angle rotor in a Sorvall centrifuge (Thermo Scientific). *Note: It is very important at this step to ensure your centrifuge balance is equivalent in mass to that of the sonicated lysate.* Cell lysates can now be analyzed.

c. Coomassie Blue Stain

After lysis, proteins are loaded and separated by a 4-20% polyacrylamide gel (Bio-Rad). Gel is then fixed in 50% MeOH, 10% AcOH, and 40% H2O for by rocking at room temperature for 30 minutes. Immediately following fixing, the gel is then stained in 50% MeOH, 10% AcOH, 39.75% H2O and 0.25% Coomassie Blue by rocking at room temperature for 5 minutes. An overnight destain is performed with 5% MeOH, 7.5% AcOH and 87.5% H2O, in which the gel should be analyzed and then can store indefinitely.

a. HA Peptide Affinity Chromatography Purification

HA resin was created by covalently linking NHS activated dry agarose resin beads (ThermoScientific) to the HA peptide (Sigma Aldrich). To create a 0.5 mL resin bed, 1 mg of HA peptide was dissolved in 1 mL of [1X] PBS pH 7.4 and coupled to 75 mg of dry agarose beads. Protocol for NHS coupling can be found: https://www.thermofisher.com/order/catalog/product/26196#/26196.

Create and pack a 0.5 mL resin bed of freshly prepared HA affinity chromatography resin in a Flex Column, equilibrated to room temperature with running buffer (Kimble). Running buffer consists of [1X] PBS, pH 7.4, .05% (v/v) TWEEN and .05% w/v sodium azide. Pour 20 mL cell lysate at a time over the resin bed carefully collecting the flowthrough. The column is washed with ≥ 300 mL running buffer before eluting the protein while simultaneously collecting flowthrough fractions. Ensure that the flow rate of running buffer does not exceed 2 mLs/min. To elute the protein from the column, 5 mL .2 M glycine at a pH of 2.2 is slowly poured over the matrix and neutralized in 1 M Tris pH 9 to yield a collected fraction at a neutral pH of 7.4. *Note: volume of the fraction is variable based entirely on preference.* Elution fractions were pooled and dialyzed overnight in PBS, pH 7.4 with SnakeSkin dialysis tubing at 4°C (Thermo Scientific). Expression is assessed by SDS-PAGE analysis on 4–20% gradient gel (Bio-Rad; Hercules, CA, USA). Protein

concentration can also be analyzed by calculating the absorbance at 280 nm and utilizing the Beer-Lambert Law.

f. Scale-up: Production of HA-ScFv (1L)

Construct used: N-terminal Light Chain gene with C-terminal His-6 tag on Heavy Chain in a pCOMB vector (ampicillin/carbenicillin resistance).

Construct name: pCOMB3H-[HA-ScFv]

The construct is newly transformed into *E. coli* XL1Blue cells or plated from a glycerol stock of freshly transformed XL1Blue cells (Stratagene; San Diego, CA, USA). The cells are plated out on LB-agar containing ampicillin (100 µg/ml) and tetracycline (15 µg/ml). Incubation then occurs overnight for 16-18 h at 37°C. A colony is selected from the plate to inoculate 1 X 5 mL LB medium containing carbenicillin (100 µg/ml), tetracycline (15 µg/ml) and dextrose (.02 M). Incubation then occurs overnight at 37°C in a shaking incubator between 220-250 RPM. At the point of overnight growth after , the 5 mL culture will then be used to inoculate 1 x 1 L Super Broth medium containing carbenicillin (100 µg/ml) and tetracycline (15 µg/ml) in a 2-L flask for appropriate aeration. After 16-18 hours, observe culture to ensure a moderate amount of growth and biofilm production. Measure the OD_{600} of culture and make note for future optimization. Ideal OD600 is approximately 1.5 A. The entire 5 mL of the overnight culture will then be used to inoculate 1 x 1 L SB broth medium containing carbenicillin (100 µg/ml) and tetracycline (15 µg/ml) in a 2 L flask for appropriate aeration. To inoculate, spin 5 mL culture at 4,000 xg for 5 minutes, pour off and discard the supernatant and vortex pellet with 1 mL of PBS. Repeat this PBS cell wash step 3 times. After discarding the final wash supernatant, 1 mL of LB is added to the pellet which is then vortexed thoroughly. The entire 1 mL of vortexed culture is then added via pipette to the 50 mLs of SB broth and swirled to mix evenly. Cultures are then grown at 37°C until mid-log phase of growth (OD_{600} is approximately 0.6 A) with a timed averaged of approximately 6 h After mid-log phase has been reached, the flask will be removed from the 37°C and placed into a 30°C

shaking incubator with equivalent RPM. Cultures are then shaken and grown overnight for 16-18 h Harvest is performed by pouring the cultures into 500 mL centrifuge bottles and spun for 20 min at 6,000 x g using a Fiberlite F13-14 x 50cy Fixed-Angle rotor in a Sorvall centrifuge (Thermo Scientific). The pellet is then washed (3 X 30 mL [1X] PBS) and recollected into a 50 mL conical tube. Store the pellet at -80°C for a minimum of 1 hour. *Note: storage time can be up to 1 year*.

Cellular lysates were produced by sonication in PBS pH 7.4 supplemented with a final concentration of 0.2 mM PMSF (Gold Biotechnology). Soluble proteins were clarified via centrifugation at 30,000× g for 30 min and filtration by 0.22 µm cellulose acetate syringe filter. Use a large probe, preferably the 300w Ultrasonic Homogenizer sonicator with the following settings: cycle 40% output power 1 minute ON and 4 minutes OFF (Vevor). Centrifugation was performed using the same Fiberlite F13-14 x 50cy Fixed-Angle rotor in a Sorvall centrifuge (Thermo Scientific). Note: It is very important at this step to ensure your centrifuge balance is equivalent in mass to that of the sonicated lysate. Cell lysate now contains solubilized HAScFv to be purified via CaptureSelect CH1-XL affinity chromatography resin (Thermo Scientific; Waltham, MA, USA).

g. Incorporated Unnatural Amino Acid Production (1 L)

Construct(s) used: N-terminal Light Chain gene with C-terminal Amber- His-6 tag on Heavy Chain preceding Ochre in a pCOMB vector (ampicillin/carbenicillin resistance).

And a tRNA/tRNA synthetase pair for the in vivo incorporation of the negatively charged unnatural amino acid, p-azido-l-phenylalanine, onto HA-ScFv heavy chain in *E. coli* response to the Amber stop codon, encoded in a pEVOL vector (chloramphenicol resistance).

Construct(s) name: pCOMB3H-HAScFv-LC-Amber-His6-Ochre and pEVOL-pAzF [1].

The constructs are newly co-transformed into *E. coli* XL1Blue cells or plated from a glycerol stock of freshly transformed XL1Blue cells (Stratagene; San Diego, CA, USA). The cells

are plated out on LB-agar containing ampicillin (100 µg/ml), tetracycline (15 µg/ml) and chloramphenicol (33 µg/ml). Incubation then occurs overnight at 37°C. A colony is selected from the plate to inoculate 1 X 10 mL LB medium containing carbenicillin (100 µg/ml), tetracycline (15 µg/ml), chloramphenicol (33 µg/ml) and a final concentration of .02 M dextrose. Incubation then occurs overnight for 18-18 h at 37°C in a shaking incubator at 220-250 RPM. The entire 10 mL of the overnight culture will then be used to inoculate 1 x 1 L SB broth medium containing carbenicillin (100 µg/ml), tetracycline (15 µg/ml) and chloramphenicol (33 µg/ml) in a 2 L flask for appropriate aeration. To inoculate, spin the 10 mL starter culture at 4,000 xg for 5 minutes, pour off and discard the supernatant and vortex pellet with 5 mL of PBS. Repeat this PBS cell wash step 3 times. After discarding the final wash supernatant, 1 mL of LB is added to the pellet which is then vortexed thoroughly. The entire 1 mL of vortexed culture is then added via pipette to the 1 L of SB broth and swirled to mix evenly. Cultures are then grown at 37°C until mid-log phase of growth (OD600 is approximately 0.6 A) which is a timed averaged of approximately 5 h After mid-log phase has been reached, 1 mM 4-Azido-L-phenylalanine (pAZF) was supplemented to the culture and expression of unnatural tRNAs and synthetase was induced with 2% (w/v) L-arabinose (Gold Biotechnology; St. Louis, MO, USA). Cultures are then shaken and grown overnight for 16-18 h Harvest is performed by pouring the cultures into 500 mL centrifuge bottles and spun for 20 min at 6,000 x g using a Fiberlite F13-14 x 50cy Fixed-Angle rotor in a Sorvall centrifuge (Thermo Scientific). The pellet is then washed (3 X 30 mL [1X] PBS) and recollected into a 50 mL conical tube. Store the pellet at -80°C for a minimum of 1 hour. *Note: storage time can be up to 1 year*. HA ScFv that successfully suppressed the amber stop codon with pAZF was purified using Nickel affinity chromatography (Gold Biotechnology) followed by purification using HA peptide affinity chromatography resin (Thermo Scientific; Waltham, MA, USA). Elution fractions were pooled and dialyzed overnight in PBS, pH 7.4. Expression was assessed by SDS-PAGE analysis on 4–20% gradient gel (Bio-Rad; Hercules, CA, USA). The final yields from 1–2 L of culture were typically in the range of 1–3 mg of HAScFv-pAzF.

h. Ni2+ Polyhistidine Affinity Chromatography Purification

Cell lysis is to be performed in Buffer A, a solution adjusted to pH 8.0 containing 20 mM HEPES, 300 mM NaCl, 300 mM KCl and 20 mM imidazole. The Ni2+ resin is then equilibrated with Buffer A and batch incubated with the lysate over ice. To batch incubate, use desired amount of resin and resuspend 1 mL Buffer A and combine with cell lysate in 50 mL conical tube and rock slowly on ice for ≥ 1 h. Using a drip column, the resin is poured slowly to pack the column while the flowthrough is collected for future analysis. Wash the column with 12 column volumes of Buffer A solution, occasionally collecting flowthrough fractions for analysis. To elute, use 5 mL Buffer A containing 250 mM imidazole, collecting 1 mL fractions in 1.5 mL Eppendorf tubes. Elution fractions were pooled and dialyzed overnight in PBS, pH 7.4 with SnakeSkin dialysis tubing at 4°C (Thermo Scientific). Expression is assessed by SDS-PAGE analysis on 4–20% gradient gel (Bio-Rad; Hercules, CA, USA). Protein concentration can also be analyzed by calculating the absorbance at 280 nm and utilizing the Beer-Lambert Law.

j. DIBO Cu-free Click Reaction

Copper-free click chemistry was performed between DIBO-QD625 (Site-Click kit, Thermo Scientific) and BG18-pAzF using a 1:1.5-fold stoichiometry, respectively. The reaction could proceed for 12–18 h at room temperature in the dark. Uncoupled DIBO-QD625 was removed from the reaction by another round of CaptureSelect CH1-XL affinity chromatography. Elution fractions were pooled and unreacted BG18-pAzF, lacking a DIBO-QD625 conjugate, was removed by filtration through a 100 Kda molecular weight cutoff filter (Site-Click kit) followed by repeated buffer exchanges with PBS, pH 7.4.

Discussion

It has been shown that SER 5 does play a role in fusion however, the mode of action is yet to be completely understood. I have created tools to investigate Env-dependent SER 5 protein-protein interactions via single particle tracking by TIRF superresolution microscopy.

Investigations of mode of actions have found several suggestions for SER 5 such as that of Env proteins from tier 2/3 isolates have been suggested to antagonize SER 5 more efficiently than *Nef* (Beitari *et al*., 2017). These strains of Env were then further studied and have shown sensitivity to SER 5 upon production in the presence of CD4 (Zhang *et al*., 2017).

Contrary to the investigation of the antagonistic method, SER 5 has been found to keep Env forced in its closed conformation. When CD4 is absent, native tier 1 Env trimers preponderantly are found to be in the open conformation, as the native tier 2/3 Env trimers preserve the closed conformation (Munro *et al*., 2017; Munro and Mathes, 2015).

Using a dual quantum dot tracking assay, Env-Env associations, SER 5-Env interactions and SER 5-Gag interactions can al all be preformed with the generated probes, BG18-QD525 Fab and anti-HA-QD605 ScFv as well as a previously generated CANTD-SkylanS (Figure 6 and Figure 11). Subcellular colocalization of all 3 proteins: Env, Gag and SER 5 can be quantified, and protein-protein interactions can be easily observed with single particle tracking. The two quantum dot probes, BG18 Fab and anti-HA ScFv are advantageous for many reasons however, their brightness and direct antigen binding specificity allow for the measure of precise and accurate direct interactions between the two proteins of interest—Env and SER 5.

Because CD4 is also a key player in Env conformation, if the recombinant production of CD4 is to be successful, the various levels of CD4 required for Env sensitivity to SER 5 can also be investigated upon the application of single particle tracking. Gag is another component needed at sites of assembly for HIV-1 replication, and there are currently no investigations reporting SER 5 interactions with Gag (Buttler *et al*., 2018). Therefore, it is possible that SER 5 could potentially serve as an antiviral host factor at the site of viral assembly.

The results obtained from the production of a dual quantum dot single particle tracking assay will yield important findings and suggestions for understanding the unknown Env-dependent or Gag-dependent SER 5 host anti-viral mode of action. My hypothesis parallels that of a recent finding that SER 5 disrupts the clustering of Env trimers (Firrito *et al.,* 2018). If the clustering of Env trimers are disrupted, then the required interactions between Env and Gag downstream would also become disrupted. A disruption between Gag and Env would thereby explain an antiviral mechanism of action of SER 5 to be that of assembly disruption.

Overall, more effort is needed to comprehend protein interactions of Ser 5, Env, Gag and even CD4 to better understand the host antiviral restriction factor, Ser 5.

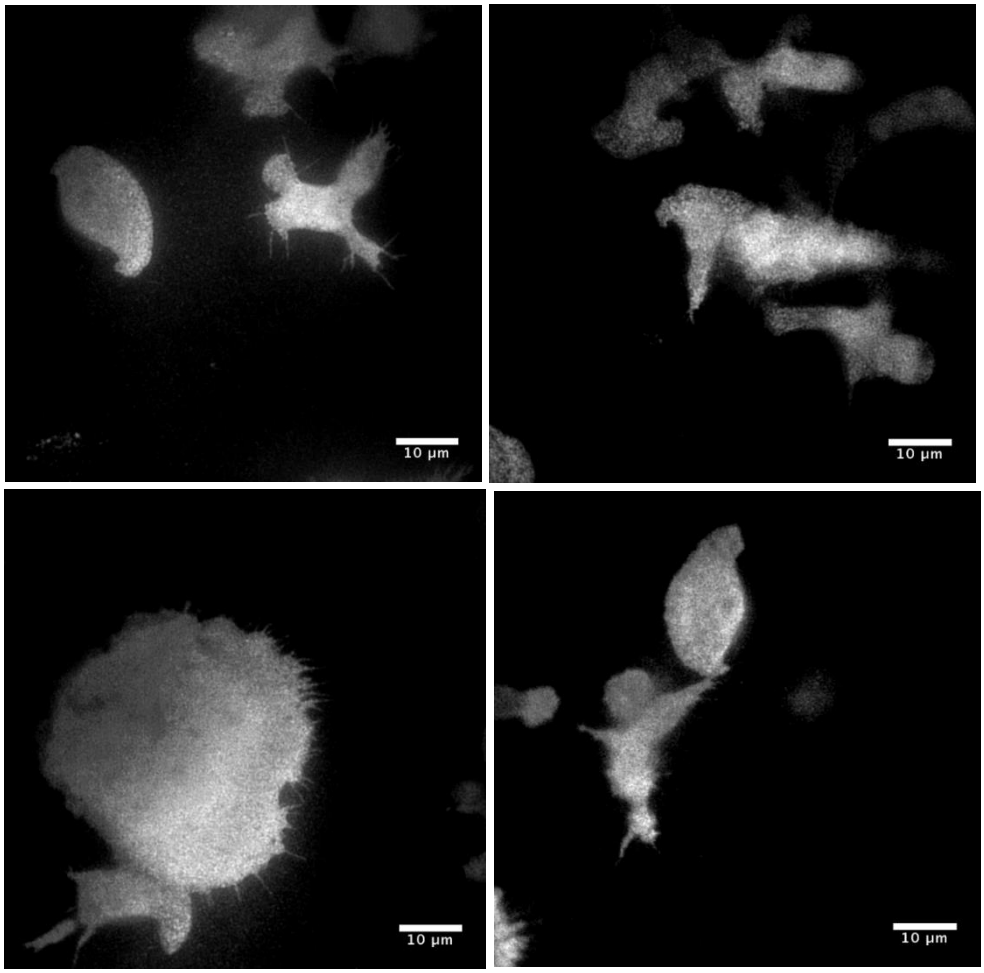

Figure 4.1. Figure 10. Native baseline expression of SER 5 on the surface of SER 5 iHAknock-in Jurkat cells

Representative image of whole Jurkat cells producing an extracellular HA epitope on SER 5. SER 5 was detected via anti HA-Atto565 ScFv and fixed and labeled for surface-exposed SER 5. Scale bars are 10 µm.

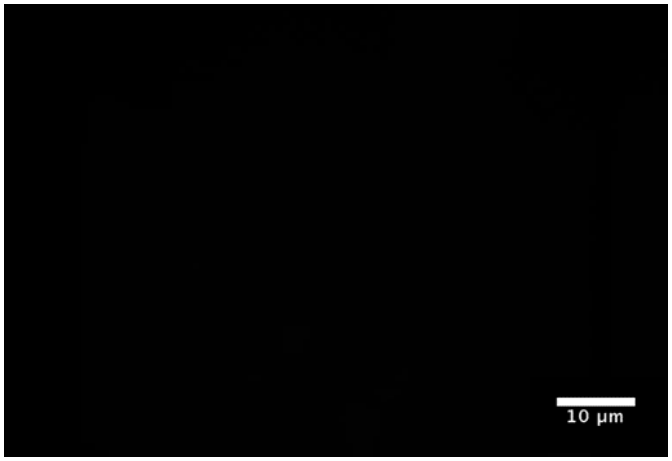

Figure 4.2. Native Jurkat cells stained with the *anti*-HA ScFv-Atto565 probe.

Negative control for immunostaining with the *anti*-HA ScFv-Atto565 fluorescent probe. Images of stained and fixed Jurkat cells. Scale bar = 10 µm.

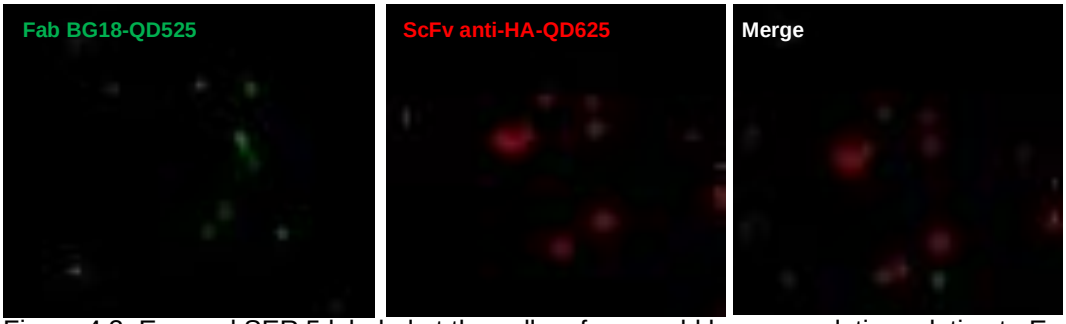

Figure 4.3. Env and SER 5 labeled at the cell surface could have correlation relative to Env diffusion.

Fixed Jurkat cells expressing WT-Env and iHA knock-ins were labeled with both anti-Env Fab BG18-QD525 (green) and anti-HA ScFv QD625 (red) and then fixed after labeling to demonstrate any Env and SER 5 correlation. In Jurkat cells, surface Env appears to have a correlation with surface SER 5.

References

1. Adamson C.; Freed E. Human immunodeficiency virus type 1 assembly, release, and maturation. *Adv Pharmacol.* **2007** , *55*, 347-387.

2. Alfadhli, A.; Still, A.; Barklis, E. Analysis of Human Immunodeficiency Virus Type 1 Matrix Binding to Membranes and Nucleic Acids. *J. Virol.* **2009**, *83*, 12196–12203.

3. *And The Band Played On,* Randy Shilts, p. 227, St. Martin's Press, 2007, ISBN 0-312-37463-1

4. Ambrose, Z.; Aiken, C. HIV-1 uncoating: connection to nuclear entry and regulation by host proteins *Virology* **2014,** *454-455*, 371–379.

5. Arts, E.; Hazuda D. HIV-1 Antiretroviral Drug Therapy. *Cold Spring Harb Perspect Med* **2012**, *2*, a007161.

6. Barbas, C.F.; Hu, D.; Dunlop, N.; Sawyer, L.; Cababa, D.; Hendry, R.M.; Nara, P.L.; Burton, D.R. In vitro evolution of a neutralizing human antibody to human immunodeficiency virus type 1 to enhance affinity and broaden strain cross-reactivity. *Proc. Natl. Acad. Sci. USA* **1994**, *91*, 3809–3813.

7. Barnes, C.O.; Gristick, H.B.; Freund, N.T.; Escolano, A.; Lyubimov, A.Y.; Hartweger, H.; West, A.P.; Cohen, A.E.; Nussenzweig, M.C.; Bjorkman, P.J. Structural characterization of a highly-potent V3-glycan broadly neutralizing antibody bound to natively-glycosylated HIV-1 envelope. *Nat. Commun.* **2018**, *9*, 1251.

8. Barré-Sinoussi, F.; Chermann, J.; Rey, F.; Nugeyre, M.; Chamaret, S.; Gruest, J.; Dauguet, C,; Axler-Blin, C.; Vézinet-Brun, F.; Rouzioux, C.; Rozenbaum, W.; Montagnier, L. Isolation of a T-lymphotropic retrovirus from a patient at risk for acquired immune deficiency syndrome (AIDS). *Science*. **1983,** 220, 868-871.

9. Bates, M.; Jones, S.; Zhuang, X. Stochastic optical reconstruction microscopy (STORM): A method for superresolution fluorescence imaging. *Cold Spring Harb. Protoc*. **2013**, *8*, 498–520.

10. Betzig, E.; Patterson, G.H.; Sougrat, R.; Lindwasser, O.W.; Olenych, S.; Bonifacino, J.S.; Davidson, M.W.; Lippincott-Schwartz, J.; Hess, H.F. Imaging intracellular fluorescent proteins at nanometer resolution. *Science* **2006**, *313*, 1642–1645.

11. Beitari, S.; Ding, S.; Pan, Q.; Finzi, A.; Liang, C. Effect of HIV-1 Env on SERINC5 antagonism. J *Virol* **2017,** *91*, 2214-2216.

12. Boutant, E.; Bonzi, J.; Anton, H.; Nasim, M.B.; Cathagne, R.; Réal, E.; Dujardin, D.; Carl, P.; Didier, P.; Paillart, J.C.; et al. Zinc Fingers in HIV-1 Gag Precursor Are Not Equivalent for gRNA Recruitment at the Plasma Membrane. *Biophys. J.* **2020**, *119*, 419–433.

13. Briggs, J.A.; Wilk, T.; Welker, R.; Kräusslich, H.G.; Fuller, S.D. Structural organization of authentic, mature HIV-1 virions and cores. *EMBO J.* **2003**, *22*, 1707–1715.

14. Buttler, C.A.; Pezeshkian, N.; Fernandez, M.V.; Aaron, J.; Norman, S.; Freed, E.O.; Van Engelenburg, S.B. Single molecule fate of HIV-1 envelope reveals late-stage viral lattice incorporation. *Nat. Commun.* **2018**, *9*.

15. Byland, R.; Vance, P.J.; Hoxie, J.A.; Marsh, M. A Conserved Dileucine Motif Mediates Clathrin and AP-2–dependent Endocytosis of the HIV-1 Envelope Protein. *Mol. Biol. Cell* **2007**, *18*, 414–425.

16. Caskey, M,; Schoofs, T.; Gruell, H.; Settler, A.; Karagounis, T.; Kreider EF.; Murrell B, Pfeifer N, Nogueira L, Oliveira TY, Learn GH, Cohen YZ, Lehmann C, Gillor D, Shimeliovich I, Unson-O'Brien C, Weiland D, Robles A, Kümmerle T, Wyen C, Levin R, Witmer-Pack M, Eren K, Ignacio C, Kiss S, West AP Jr, Mouquet H, Zingman BS, Gulick RM, Keler T, Bjorkman PJ, Seaman MS, Hahn BH, Fätkenheuer G, Schlesinger SJ,

Nussenzweig, M.; Klein, F. Antibody 10-1074 suppresses viremia in HIV-1-infected individuals. *Nat Med*. **2017 ,***23*, 185-191.

17. “CDC's HIV Work Saves Lives and Money Infographics.” Centers for Disease Control and Prevention, Centers for Disease Control and Prevention, 6 Feb. 2020, www.cdc.gov/nchhstp/budget/infographics/hiv.html.

18. Checkley, M.A.; Luttge, B.G.; Freed, E.O. HIV-1 envelope glycoprotein biosynthesis, trafficking, and incorporation. *J. Mol. Biol.* **2011**, *410*, 582–608.

19. Chen, J.; Grunwald, D.; Sardo, L.; Galli, A.; Plisov, S.; Nikolaitchik, O.; Chen, D.; Lockett, S.; Larson, D.; Pathak, V.; et al. Cytoplasmic HIV-1 RNA is mainly transported by diffusion in the presence or absence of Gag protein*. Proc. Natl. Acad. Sci.* **2014 ,** *111*, E5205–E5213.

20. Chin, J.; Santoro, S.; Martin, A.; King, D.; Wang, L., Schultz, P. Addition of p-azido-L-phenylalanine to the genetic code of Escherichia coli. *J Am Chem Soc.* **2002**, *124*, 9026-9027.

21. Choe, H.; Farzan, M.; Sun, Y.; Sullivan, N.; Rollins, B.; Ponath, P. D.; Wu, L.; Mackay, C.; LaRosa, G.; Newman, W.; Gerard, N.; Gerard, C.; Sodroski, J. The beta-chemokine receptors CCR3 and CCR5 facilitate infection by primary HIV-1 isolates. *Cell* **1996** , 85, 1135-1148.

22. Chojnacki, J. Eggeling, C. Super-resolution fluorescence microscopy studies of human immunodeficiency virus. *Retrovirology* **2018** ,*15,* 41.

23. Chojnacki, J.; Staudt, T.; Glass, B.; Bingen, P.; Engelhardt, J.; Anders, M.; Schneider, J.; Müller, B.; Hell, S.W.; Kräusslich, H.G. Maturation-dependent HIV-1 surface protein redistribution revealed by fluorescence nanoscopy. *Science* **2012**, *338*, 524–528.

24. Chojnacki, J.; Waithe, D.; Carravilla, P.; Huarte, N.; Galiani, S.; Enderlein, J.; Eggeling, C. Envelope glycoprotein mobility on HIV-1 particles depends on the virus maturation state. *Nat. Commun.* **2017**, *8*.

25. Crocker, J.C.; Grier, D.G. Methods of digital video microscopy for colloidal studies. *J. Colloid Interface Sci.* **1996**, *179*, 298–310.

26. Doores, K. J. et al. Two classes of broadly neutralizing antibodies within a single lineage directed to the high-mannose patch of HIV envelope. *J. Virol.* **2015**, *89*, 1105–1118.

27. Ettinger, A. & Wittmann, T. Fluorescence Live Cell Imaging. doi:10.1016/B978-0-12-420138-5.00005-7.

28. Ferrari, R.; Manfroi, A.; Young, W. Strongly and weakly self-similar diffusion. *Phys. Nonlinear Phenom.* **2001**, *154*, 111–137.

29. Floderer, C.; Masson, J.B.; Boilley, E.; Georgeault, S.; Merida, P.; El Beheiry, M.; Dahan, M.; Roingeard, P.; Sibarita, J.B.; Favard, C.; et al. Single molecule localisation microscopy reveals how HIV-1 Gag proteins sense membrane virus assembly sites in living host CD4 T cells. *Sci. Rep.* **2018**, *8*, 1–15.

30. Fogarty, K.H.; Berk, S.; Grigsby, I.F.; Chen, Y.; Mansky, L.M.; Mueller, J.D. Interrelationship between cytoplasmic retroviral Gag concentration and Gag–membrane association. *J. Mol. Biol.* **2014**, *426*, 1611–1624.

31. Freund, N.T.; Wang, H.; Scharf, L.; Nogueira, L.; Horwitz, J.A.; Bar-On, Y.; Golijanin, J.; Sievers, S.A.; Sok, D.; Cai, H.; et al. Coexistence of potent HIV-1 broadly neutralizing antibodies and antibody-sensitive viruses in a viremic controller. *Sci. Transl. Med.* **2017**, *9*, 1–14.

32. Firrito, C.; Bertelli, C.; Vanzo, T.; Chande, A.; Pizzato, M. SERINC5 as a new restriction factor for human immunodeficiency virus and murine leukemia virus. *Annu Rev Virol* **2018** ,*5,* 323–340.

33. Furuta, R.; Wild, C.; Weng, Y. *et al.* Capture of an early fusion-active conformation of HIV-1 gp41. *Nat Struct Mol Biol* **1998** , *5*, 276–279.

34. Gallo, C.; Salahuddin, S.; Popovic, M.; Shearer, G.; Kaplan, M.;, Haynes, B.; Palker, J.; Redfield, R.; Oleske, J.; Safai, B.; et al. Frequent detection and isolation of cytopathic retroviruses (HTLV-III) from patients with AIDS and at risk for AIDS. Science **1984,** *224*, 500-503.

35. Gamble, T.R.; Yoo, S.; Vajdos, F.F.; von Schwedler, U.K.; Worthylake, D.K.; Wang, H.; McCutcheon, J.P.; Sundquist, W.I.; Hill, C.P. Structure of the carboxyl-terminal dimerization domain of the HIV-1 capsid protein. *Science* **1997**, *278*, 849–853.

36. Garces, F. et al. Affinity maturation of a potent family of HIV antibodies is primarily focused on accommodating or avoiding glycans. *Immunity* **2015***, 43*, 1053–1063.

37. “Global HIV & AIDS Statistics - 2020 Fact Sheet.” UNAIDS, Jan. 2021, www.unaids.org/en/resources/fact-sheet.

38. Gray, R.D.; Beerli, C.; Pereira, P.M.; Scherer, K.M.; Samolej, J.; Bleck, C.K.E.; Mercer, J.; Henriques, R. VirusMapper: open-source nanoscale mapping of viral architecture through super-resolution microscopy. *Sci. Rep.* **2016**, *6*, 29132.

39. Gristick, H. B. et al. Natively glycosylated HIV-1 Env structure reveals new mode for antibody recognition of the CD4-binding site. *Nat. Struct. Mol. Biol.* **2016**, *23,* 906–915.

40. Gunzenhäuser, J.; Olivier, N.; Pengo, T.; Manley, S. Quantitative super-resolution imaging reveals protein stoichiometry and nanoscale morphology of assembling HIV-Gag virions. *Nano Lett.* **2012**, *12*, 4705–4710.

41. Han, J.J.; Kunde, Y.; Hong-Geller, E.; Werner, J.H. Actin restructuring during Salmonella typhimurium infection investigated by confocal and super-resolution microscopy. *J. Biomed. Opt.* **2014**, *19*, 016011.

42. Hell, S.W. Far-field optical nanoscopy. *Science* **2007**, *316*, 1153–1158.

43. Helma, J.; Schmidthals, K.; Lux, V.; Nüske, S.; Scholz, A.M.; Kräusslich, H.G.; Rothbauer, U.; Leonhardt, H. Direct and Dynamic Detection of HIV-1 in Living Cells. *PLoS ONE* **2012**, *7*, e50026.

44. Hendrix, J.; Baumgärtel, V.; Schrimpf, W.; Ivanchenko, S.; Digman, M.A.; Gratton, E.; Kräusslich, H.G.; Müller, B.; Lamb, D.C. Live-cell observation of cytosolic HIV-1 assembly onset reveals RNA-interacting Gag oligomers. *J. Cell Biol.* **2015**, *210*, 629–646.

45. Hess, S.T.; Girirajan, T.P.; Mason, M.D. Ultra-high resolution imaging by fluorescence photoactivation localization microscopy. *Biophys. J.* **2006**, *91*, 4258–4272.

46. Hess, S.T.; Gould, T.J.; Gudheti, M.V.; Maas, S.A.; Mills, K.D.; Zimmerberg, J. Dynamic clustered distribution of hemagglutinin resolved at 40 nm in living cell membranes discriminates between raft theories. *Proc. Natl. Acad. Sci. USA* **2007**, *104*, 17370–17375.

47. Horsington, J.; Lynn, H.; Turnbull, L.; Cheng, D.; Braet, F.; Diefenbach, R.J.; Whitchurch, C.B.; Karupiah, G.; Newsome, T.P. A36-dependent actin filament nucleation promotes release of vaccinia virus. *PLoS Pathog.* **2013**, *9*, e1003239.

48. Huang, F.; Hartwich, T.M.; Rivera-Molina, F.E.; Lin, Y.; Duim, W.C.; Long, J.J.; Uchil, P.D.; Myers, J.R.; Baird, M.A.; Mothes, W.; et al. Video-rate nanoscopy using sCMOS camera–specific single-molecule localization algorithms. *Nat. Methods* **2013**, *10*, 653–658.

49. Inavalli, V.V.; Lenz, M.O.; Butler, C.; Angibaud, J.; Compans, B.; Levet, F.; Tønnesen, J.; Rossier, O.; Giannone, G.; Thoumine, O.; et al. A super-resolution platform for correlative live single-molecule imaging and STED microscopy. *Nat. Methods* **2019**, *16*, 1263–1268.

50. Iliopoulou, M.; Nolan, R.; Alvarez, L.; Watanabe, Y.; Coomer, C.; Jakobsdottir, G.; Bowden, T.; Padilla-Parra, S. A dynamic three-step mechanism drives the HIV-1 pre-fusion reaction. *Nat Struct Mol Biol*. **2018** ,*9*, 814-822.

51. Inamdar, K.; Floderer, C.; Favard, C.; Muriaux, D. Monitoring HIV-1 Assembly in Living Cells: Insights from Dynamic and Single Molecule Microscopy. *Viruses*. **2019** ,*1*, 72.

52. Ivanchenko, S.; Godinez, W.J.; Lampe, M.; Kräusslich, H.G.; Eils, R.; Rohr, K.; Bräuchle, C.; Müller, B.; Lamb, D.C. Dynamics of HIV-1 assembly and release. *PLoS Pathog.* **2009**, *5*.

53. Jaffe, W.; Bregman J.; Selik M. Acquired immune deficiency syndrome in the United States: the first 1,000 cases*. J Infect Dis.* **1983,** *2*, 339-345.

54. Jouvenet, N.; Bieniasz, P.D.; Simon, S.M. Imaging the biogenesis of individual HIV-1 virions in live cells. *Nature* **2008**, *454*, 236–240.

55. Kitchen, L.; Barin, F.; Sullivan, J.; McLane, M.; Brettler, D.; Levine, P.; Essex, M. Aetiology of AIDS—antibodies to human T-cell leukaemia virus (type III) in haemophiliacs. *Nature* **1984**, *312*, 367–369.

56. Lakowicz, J. R. (2006). Principles of fluorescence spectroscopy (3rd ed). New York: Springer

57. Laine, R.F.; Albecka, A.; Van De Linde, S.; Rees, E.J.; Crump, C.M.; Kaminski, C.F. Structural analysis of herpes simplex virus by optical super-resolution imaging. *Nat. Commun.* **2015**, *6*, 1–10.

58. Lehmann, M.; Rocha, S.; Mangeat, B.; Blanchet, F.; Uji-i, H.; Hofkens, J.; Piguet, V. Quantitative multicolor super-resolution microscopy reveals tetherin HIV-1 interaction. *PLoS Pathog.* **2011**, *7*, e1002456.

59. Li, S.; Hill, C.P.; Sundquist, W.I.; Finch, J.T. Image reconstructions of helical assemblies of the HIV-1 CA protein. *Nature* **2000**, *407*, 409–413.

60. Liu, Q.; Chen, L.; Aguilar, H.C.; Chou, K.C. A stochastic assembly model for Nipah virus revealed by super-resolution microscopy. *Nat. Commun.* **2018**, *9*, 1–7.

61. Mailler E.; Bernacchi S.; Marquet R.; Paillart J.; Vivet-Boudou V.; Smyth R. The life-cycle of the HIV-1 gag–RNA complex. *Viruses* **2016** , *8*.

62. Melikyan G.; Markosyan R.; Hemmati H.; Delmedico M.; Lambert D.; Cohen F. Evidence that the transition of HIV-1 gp41 into a six-helix bundle, not the bundle configuration, induces membrane fusion. *J Cell Biol* **2000,** *151*, 413–423.

63. Mouquet, H.; Scharf, L.; Euler, Z.; Liu, Y.; Eden, C.; Scheid, J.; Halper-Stromberg, A.; Gnanapragasam P.; Spencer, D.; Seaman, M.; Schuitemaker, H.; Feizi, T.; Nussenzweig, M.; Bjorkman, P. Complex-type N-glycan recognition by potent broadly neutralizing HIV antibodies. *Proc Natl Acad Sci USA*. **2012**, *109,* E3268–E3277.

64. Munro, J.; Gorman, J.; Ma, X.; Zhou, Z.; Arthos, J.; Burton, D.; Koff, W.; Courter, J.; Smith, A III.; Kwong, P.; Blanchard, S.; Mothes, W. Conformational dynamics of single HIV-1 envelope trimers on the surface of native virions. *Science* **2014,** *346,* 759–763.

65. Munro, J.; Mothes, W. Structure and dynamics of the native HIV-1 Env trimer. *J Virol* **2015,** 89, 5752–5755.

66. Muranyi, W.; Malkusch, S.; Müller, B.; Heilemann, M.; Kräusslich, H.G. Super-Resolution Microscopy Reveals Specific Recruitment of HIV-1 Envelope Proteins to Viral Assembly Sites Dependent on the Envelope C-Terminal Tail. *PLoS Pathog.* **2013**, *9*.

67. Ono, A.; Ablan, S.D.; Lockett, S.J.; Nagashima, K.; Freed, E.O. HIV-1 Gag targeting to the plasma membrane. *October* **2004**, *101*, 2–7.

68. Olety, B.; Ono, A. Roles played by acidic lipids in HIV-1 Gag membrane binding*. Virus Res*. **2014** ,*193,* 108–115.

69. Pawley J. ed. Handbook of biological confocal microscopy. **2006** Springer, New York.

70. Pereira, C.F.; Rossy, J.; Owen, D.M.; Mak, J.; Gaus, K. HIV taken by STORM: Super-resolution fluorescence microscopy of a viral infection. *Virol. J.* **2012**, *9*, 84.

71. Pejchal, R. et al. A potent and broad neutralizing antibody recognizes and penetrates the HIV glycan shield. *Science* **2011**, *334*, 1097–1103.

72. Pezeshkian, N.; Groves, N.; van Engelenburg, S. Single-molecule imaging of HIV-1 envelope glycoprotein dynamics and Gag lattice association exposes determinants responsible for virus incorporation. *Proc. Natl. Acad. Sci. USA* **2019**, *116*.

73. Pier, G.; Lyczak, J.; Wetzler, L.; Ruebush, M. Immunology, infection, and immunity. **2004** 1st ed. Washington, D.C.: *ASM Press.*

74. Pollard, V; Malim, M. The HIV-1 Rev Protein. *Annu. Rev. Microbiol.* **1998** , *52*, 491–532.

75. Pomerantz, R.; Horn, L. Twenty years of therapy for HIV-1 infection. *Nat. Med.* **2003**, *7*, 867–873.

76. Popovic, M.; Sarngadharan, M.; Read, E.; Gallo, C. Detection, isolation, and continuous production of cytopathic retroviruses (HTLV-III) from patients with AIDS and pre-AIDS. *Science* **1984,** *224*, 497-500.

77. Purcell, D; Martin, M. Alternative splicing of human immunodeficiency virus type 1 mRNA modulates viral protein expression, replication, and infectivity. *J. Virol*. **1993,** *67*, 6365–6378.

78. Qian, H.; Sheetz, M.P.; Elson, E.L. Single particle tracking. Analysis of diffusion and flow in two-dimensional systems. *Biophys. J.* **1991**, *60*, 910–921.

79. Richman, D. HIV chemotherapy. *Nature* **2001**, *410*, 995–1001.

80. Rothenberg, R.; Woelfel, M.; Stoneburner, R.; Milberg, J.; Parker, R.; Truman, B. Survival with the Acquired Immunodeficiency Syndrome. *New Eng J of Med* **1987,** *21*, 1297–1302.

81. Roy, N.H.; Chan, J.; Lambelé, M.; Thali, M. Clustering and mobility of HIV-1 Env at viral assembly sites predict its propensity to induce cell-cell fusion. *J. Virol.* **2013**, *87*, 7516–7525.

82. Rust, M.J.; Bates, M.; Zhuang, X. Sub-diffraction-limit imaging by stochastic optical reconstruction microscopy (STORM). *Nat. Methods* **2006**, *3*, 793–796.

83. Saad, J.S.; Miller, J.; Tai, J.; Kim, A.; Ghanam, R.H.; Summers, M.F. Structural basis for targeting HIV-1 Gag proteins to the plasma membrane for virus assembly. *Proc. Natl. Acad. Sci. USA* **2006**, *103*, 11364–11369.

84. Sakin, V.; Hanne, J.; Dunder, J.; Anders-Össwein, M.; Laketa, V.; Nikić, I.; Kräusslich, H.G.; Lemke, E.A.; Müller, B. A Versatile Tool for Live-Cell Imaging and Super-Resolution Nanoscopy Studies of HIV-1 Env Distribution and Mobility. *Cell Chem. Biol.* **2017**, *24*, 635.e5–645.e5.

85. Schermelleh, L.; Carlton, P.M.; Haase, S.; Shao, L.; Winoto, L.; Kner, P.; Burke, B.; Cardoso, M.C.; Agard, D.A.; Gustafsson, M.G.; et al. Subdiffraction multicolor imaging of the nuclear periphery with 3D structured illumination microscopy. *Science* **2008**, *320*, 1332–1336.

86. Shroff, H.; Galbraith, C.G.; Galbraith, J.A.; Betzig, E. Live-cell photoactivated localization microscopy of nanoscale adhesion dynamics. *Nat. Methods* **2008**, *5*, 417–423.

87. Siegal, P; Lopez, C.; Hammer, S.; Brown, E.; Kornfeld, S.; Gold, J.; Hassett, J.; Hirschman, S.; Cunningham-Rundles, C.; Adelsberg, B.; Parham, O.; Siegal, M.; Cunningham-Rundles, S.; Armstrong, D. Severe acquired immunodeficiency in male homosexuals, manifested by chronic perianal ulcerative herpes simplex lesions. *N Engl J Med* **1981**, 305, 1439-1444.

88. Sigal Y.; Zhou R.; Zhuang X. Visualizing and discovering cellular structures with super-resolution microscopy. *Science*. **2018**, 361, 880-887.

89. Simonson, P.; Rothenberg, E.; Selvin, P. Single-molecule-based super-resolution images in the presence of multiple fluorophores. *Nano Lett* **2011**, *11*, 5090–5096.

90. Sok, D. et al. A prominent site of antibody vulnerability on HIV envelope incorporates a motif associated with CCR5 binding and its camouflaging glycans. *Immunity* **2016,** *45*, 31–45.

91. Stahl, E.; Friedman-Kien, R.; Dubin, M.; Marmor; Zolla-Pazner, S. Immunologic abnormalities in homosexual men. *Am. J. Med*. **1982,** *73*, 171-178.

92. Steichen, J.; Lin, Y.; Havenar-Daughton, C.; Pecetta, S.; Ozorowski, G.; Willis, J.; Toy, L.; Sok, D.; Liguori, A.; Kratochvil, S.; Torres, J.; Kalyuzhniy, O.; Melzi, E.; Kulp, D.; Raemisch, S.; Hu, X.; Bernard, S.; Georgeson, E.; Phelps, N.; Adachi, Y.; Kubitz, M.; Landais, E.; Umotoy, J.; Robinson, A.; Briney, B.; Wilson, I.; Burton DR, Ward AB, Crotty S, Batista FD, Schief WR. A generalized HIV vaccine design strategy for priming of broadly neutralizing antibody responses. *Science*. **2019,** *366,* 4380.

93. Strickland, M.; Ehrlich, L.; Watanabe, S.; Khan, M.; Strub, M.; Luan, C.; Carter, C. Tsg101 chaperone function revealed by HIV-1 assembly inhibitors. *Nat Comm* **2017** , *8,* 1391.

94. Sundquist W.; Kräusslich H. HIV-1 assembly, budding, and maturation. *Cold Spring Harb. Perspect. Med.* **2012** , *2,* a006924.

95. Tam, J.; Cordier, G.; Borbely, J.; Álvarez, Á.; Lakadamyali, M. Cross-talk-free multi-color storm imaging using a single fluorophore. *PLoS One* **2014** ,*9.*

96. Tremblay, M.; Rooke, R.; Geleziunas, R.; Wainberg, M.A.; Sullivan, A.K.; Tsoukas, C.; Gilmore, N.; Shematek, G. New cd4 (+) cell line susceptible to infection by hiv-1. *J. Med. Virol.* **1989**, *28*, 243–249.

97. Thompson, R.; Larson D.; Webb W. Precise nanometer localization analysis for individual fluorescent probes. *Biophys J.* 2002*, 82,* 2775–2783.

98. Turner, B.; Summers, M. Structural Biology of HIV. *J. Mol. Biol.* **1999**, *285*, 1-32.

99. Van Engelenburg, S.B.; Shtengel, G.; Sengupta, P.; Waki, K.; Jarnik, M.; Ablan, S.D.; Freed, E.O.; Hess, H.F.; Lippincott-Schwartz, J. Distribution of ESCRT machinery at HIV assembly sites reveals virus scaffolding of ESCRT subunits. *Science* **2014**, *343*, 653–656.

100. Veronese, F.; DeVico, A.; Copeland, T.; Oroszlan, S.; Gallo, R.; Sarngadharan M. Characterization of gp41 as the transmembrane protein coded by the HTLV-III/LAV envelope gene. *Science* **1985** , *27*, 1402-1405.

101. Vira S.; Mekhedov, E.; Humphrey, G.; Blank, P. Fluorescent-labeled antibodies: Balancing functionality and degree of labeling. *Anal. Biochem.* **2010,** 402, 146-150.

102. Walker, L. M. et al. Broad neutralization coverage of HIV by multiple highly potent antibodies. Nature **2011**, 477, 466–470.

103. Yacoob, C.; Pancera, M.; Vigdorovich, V.; Oliver, B.; Glenn J.; Feng J.; Sather D.; McGuire, A.; Stamatatos L. Differences in Allelic Frequency and CDRH3 Region Limit the

Engagement of HIV Env Immunogens by Putative VRC01 Neutralizing Antibody Precursors. Cell Rep **2016** ,17, 1560-1570.

104. Zhang, X.; Chen, X.; Zeng, Z.; Zhang, M.; Sun, Y.; Xi, P.; Peng, J.; Xu, P. Development of a reversibly switchable fluorescent protein for super-resolution optical fluctuation imaging (SOFI). ACS Nano **2015**, 9, 2659–2667.

105.Zhang, X.; Shi, J.; Qiu, X.; Chai, Q.; Frabutt, D.; Schwartz, R.; Zheng, Y. CD4 Expression and Env Conformation Are Critical for HIV-1 Restriction by SERINC5. J. of virology **2019** ,93, 544.

106. Zhang, Y.; Lara-Tejero, M.; Bewersdorf, J.; Galán, J.E. Visualization and characterization of individual type III protein secretion machines in live bacteria. Proc. Natl. Acad. Sci. USA **2017**, 114, 6098–6103.